AFRL-ML-WP-TR-2004-4291

MIXED ANION HETEROSTRUCTURE MATERIALS

Gary S. May and Z. L. Wang

Georgia Tech Research Corporation
Georgia Institute of Technology
400 Tenth Street
Atlanta, GA 30332-0245

April S. Brown

Duke University

OCTOBER 2004

Final Report for 06 June 1998 – 30 June 2004

STINFO FINAL REPORT

MATERIALS AND MANUFACTURING DIRECTORATE
AIR FORCE RESEARCH LABORATORY
AIR FORCE MATERIEL COMMAND
WRIGHT-PATTERSON AIR FORCE BASE, OH 45433-7750

NOTICE

Using Government drawings, specifications, or other data included in this document for any purpose other than Government procurement does not in any way obligate the U.S. Government. The fact that the Government formulated or supplied the drawings, specifications, or other data does not license the holder or any other person or corporation; or convey any rights or permission to manufacture, use, or sell any patented invention that may relate to them.

This report was cleared for public release by the Air Force Research Laboratory Wright Site Public Affairs Office (AFRL/WS) and is releasable to the National Technical Information Service (NTIS). It will be available to the general public, including foreign nationals.

THIS TECHNICAL REPORT IS APPROVED FOR PUBLICATION.

/s/

WILLIAM C. MITCHEL, Project Engineer
Sensor Materials Branch
Survivability & Sensor Materials Division

/s/

LAURA S. REA, Chief
Sensor Materials Branch
Survivability & Sensor Materials Division

/s/

KATHERINE A. STEVENS, Chief
Survivability & Sensor Materials Division
Materials & Manufacturing Directorate

This report is published in the interest of scientific and technical information exchange and its publication does not constitute the Government's approval or disapproval of its ideas or findings.

REPORT DOCUMENTATION PAGE

Form Approved
OMB No. 0704-0188

1. REPORT DATE *(DD-MM-YY)*	2. REPORT TYPE	3. DATES COVERED *(From - To)*
October 2004	Final	06/06/1998 – 06/30/2004

4. TITLE AND SUBTITLE
MIXED ANION HETEROSTRUCTURE MATERIALS

5a. CONTRACT NUMBER
F33615-98-C-5428

5b. GRANT NUMBER

5c. PROGRAM ELEMENT NUMBER
62102F

6. AUTHOR(S)
Gary S. May and Z. L. Wang (GTRC)
April S. Brown (Duke University)

5d. PROJECT NUMBER
4348

5e. TASK NUMBER
71

5f. WORK UNIT NUMBER
13

7. PERFORMING ORGANIZATION NAME(S) AND ADDRESS(ES)

Georgia Tech Research Corp.
Georgia Institute of Technology
400 Tenth Street
Atlanta, GA 30332-0245

Duke University

8. PERFORMING ORGANIZATION REPORT NUMBER

9. SPONSORING/MONITORING AGENCY NAME(S) AND ADDRESS(ES)
Materials and Manufacturing Directorate
Air Force Research Laboratory
Air Force Materiel Command
Wright-Patterson AFB, OH 45433-7750

10. SPONSORING/MONITORING AGENCY ACRONYM(S)
AFRL/MLPS

11. SPONSORING/MONITORING AGENCY REPORT NUMBER(S)
AFRL-ML-WP-TR-2004-4291

12. DISTRIBUTION/AVAILABILITY STATEMENT
Approved for public release; release is unlimited.

13. SUPPLEMENTARY NOTES
Report contains color.

14. ABSTRACT

Inhibition of anion exchange reactions during molecular beam epitaxy is critical to the synthesis of mixed-anion heterojunction interfaces. These interfaces are the basic structural building blocks of advanced electronic and optoelectronic devices that are critical to DoD applications. Anion exchange is a key surface and subsurface reaction leading to interfacial intermixing. Other related reactions include segregation, diffusion, and clustering. Interfacial intermixing results in uncontrolled strain and related bandstructure modifications that degrade device performance, reliability, and manufacturability. This project represents a study, both experimentally and theoretically, of the fundamental structural properties and process conditions that drive anion exchange and related reactions. Our techniques are applied to As-, P-, and Sb-based mixed anion heterostructures, as well as to enable the control of anion exchange to Sb/As device materials.

15. SUBJECT TERMS
molecular beam epitaxy, heterostructures, antimonides, phosphides

16. SECURITY CLASSIFICATION OF:			17. LIMITATION OF ABSTRACT:	18. NUMBER OF PAGES	19a. NAME OF RESPONSIBLE PERSON (Monitor)
a. REPORT	b. ABSTRACT	c. THIS PAGE			
Unclassified	Unclassified	Unclassified	SAR	56	William C. Mitchel 19b. TELEPHONE NUMBER *(Include Area Code)* (937) 255-4474 x3214

Standard Form 298 (Rev. 8-98)
Prescribed by ANSI Std. Z39-18

TABLE OF CONTENTS

LIST OF FIGURES

LIST OF TABLES

1. Introduction

Inhibition of anion exchange reactions during molecular beam epitaxy is critical to the synthesis of mixed-anion heterojunction interfaces. These interfaces are the basic structural building blocks of advanced electronic and optoelectronic devices that are critical to DoD applications. Anion exchange is a key surface and subsurface reaction leading to interfacial intermixing. Other related reactions include segregation, diffusion, and clustering. Interfacial intermixing results in uncontrolled strain and related bandstructure modifications that degrade device performance, reliability, and manufacturability.

During the course of this project, we have studied, both experimentally and theoretically, the fundamental structural properties and process conditions that drive anion exchange and related reactions. We have applied our techniques to As-, P-, and Sb-based mixed anion heterostructures. We have also applied advanced modelling techniques to enable the control of anion exchange to Sb/As device materials.

1.1 Key Findings

The key finds of this effort are listed below.

(1) A thermodynamic approach was developed to assess the extent of anion exchange reactions during the heteroepitaxy of dissimilar anion III-V compound semiconductor structures. We found that the extent of anion exchange can be predicted by the change in the Gibbs free energy. Bond strength changes can only be used as a guide in comparing the relative tendency for exchange, rather than as a criterion for exchange. The driving force for anion exchange strongly depends on the conditions during interface formation. A number of important factors, including bond strength, misfit strain energy, surface structure and energy, the equilibrium between dimers V_2 and tetramers V_4, and segregation, are discussed in terms of their contributions to the thermodynamics.

(2) A wide range of As/Sb, Sb/As, P/As structures exhibiting different degrees of anion exchange reactions were synthesized and fully characterized. Superlattice structures were synthesized by allowing a dissimilar anion fluxes to impinge on a binary surface. The intermixed layers are characterized using high resolution x-ray diffraction, spectroscopic ellipsometry, and x-ray photospectroscopy (XPS). The importance of substrate temperature, flux exposure time, anion surface richness (as revealed through the surface reconstruction), and incident anion molecular species was examined. Sb/As structures exhibit Sb surface segregation, and the subsequent incorporation of the segregating surface population into epitaxial overlayers. As/Sb exchange was significant and enhanced by the use of incident dimer fluxes. Competitive reactions between exchange and isoelectronic compound formation yields complex structures and dependences on the factors examined. P/As exchange was also significant and, as with the case of As/Sb, competitive reactions were found. As-rich reconstructions were found to inhibit exchange, thereby showing the importance of the surface structure to subsequent exchange. Chemical models were articulated for each of the systems.
(3) A hybrid neural network model was constructed by characterizing the growth of $GaAs_{1-y}P_y$/GaAs strained layer superlattices (SLS) grown on (001) GaAs substrates by molecular

beam epitaxy. These heterostructures were formed by the P_2 exposure of an As-stabilized GaAs surface, and *ex-situ* high-resolution x-ray diffraction (HRXRD) was performed to determine the phosphorus composition at the interfaces. A first-order kinetic model was then developed to describe the mechanisms of anion exchange, surface desorption, and diffusion. A semi-empirical hybrid neural network was used to estimate the parameters of the kinetic model and analyze the microscopic processes occurring at the interfaces of the mixed anion III-V heterostructures. The phosphorus diffusion process in GaAs was estimated to have a diffusion coefficient of $D = 7\times10^{-15} \exp(-0.11/k_B T_s)$ $cm^2 s^{-1}$ for samples with $P_{As_4} = 4\times10^{-6}$ torr and exhibited enhanced phosphorus intermixing for samples with lower As-stabilizing fluxes.

(4) The InAs-AlSb high electron mobility tTransistor (HEMT) is of critical importance for future millimeter wave and high-speed electronic devices. We have achieved record 300 K electron mobility in InAs channel structures. We applied various growth techniques to the critical mixed-anion, As/Sb, inverted interface to discover the impact on device-relevant properties.

(5) We have made new **discoveries regarding the clustering and dislocation microstructure** of GaInP-GaAs heterostructures that derive from anion exchange reactions. The information is contained in [9] and [10] in Section 4 and not included in the body of this report.

(6) In addition, while outside of the scope of our statement of work and not directly supported by this effort, we applied **exchange techniques to nanostructures** (quantum dots) to show that exchange reactions can enhance or inhibit quantum dot formation and can lead to improved vertical self-assembly.

2. Detailed Discussions

2.1 Thermodynamic Modelling

2.1.1 Basic Models

Bond strength energies are often used to predict whether anion exchange will occur or not. It is generally assumed that weaker-for-stronger-bond exchange (e.g. Sb-for-As, As-for-P, and Sb-for-P) cannot occur under typical MBE conditions [1]. However, this was proved wrong by Wang [2], who reported that up to 1 ML of As can be replaced by Sb when the As-terminated InAs (001) surface was exposed to the Sb_2-flux at a temperature of about 380 °C. As-for-P exchange was observed experimentally much earlier [3]. A detailed study showed that about two monolayers of InAs are formed on the InP (001) surface as a result of As-for-P exchange [4]. Further studies showed that As/P exchange can also occur under metal-organic vapor phase epitaxy (MOVPE) conditions [5].Our results in Section 2.2 show a range of intermixing for various conditions, as well. Apparently, bond strength cannot be generally used as the primary criteria for predicting whether or not anion exchange will occur.

We have exploited a thermodynamic approach to analyze anion exchange reactions, with a focus on the reaction driving force and direction under standard MBE conditions. A number of important factors, including bond strength, misfit strain energy, surface structure and energy, the equilibrium between dimers V_2 and tetramers V_4, and segregation, were discussed in terms of their contributions to the thermodynamics.

Fig. 2.1.1 shows a simplified model of anion exchange under MBE conditions. The surface is exposed to a V_{B2} flux with a beam equivalent pressure (BEP), P_0, or beam flux, J_0, for a unit of time. Then, the V_{B2} beam is shut off and the system is relaxed into equilibrium. After the exchange reaction, V_{B2} molecules depart the surface with a flux, J_{B2}, or BEP, P_{B2}. The exchange product for the group V species may be a mixture of V_{A2} and V_{A4} (e.g. As_2 and As_4), depending on the exchange conditions.

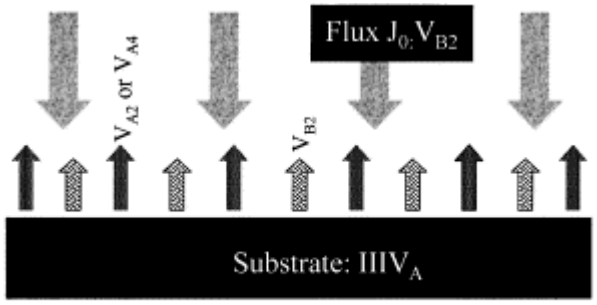

Note: the downward arrow represent the inward flux, and the upward ones the desorption flux. The thickness schematically represents the magnitude of the fluxes

Figure 2.1.1: Simplified thermodynamic model of exchange reaction.

Note that these theoretical conditions for the thermodynamics study form the basis for our experimental studies in Section 2.2 of this report. For clarity, we first consider V_{A2} only. The flux and BEP for the product gas V_{A2} are J_{A2} and P_{A2}, respectively. During exchange, the surface is assumed to remain flat, smooth, and coherent to the substrate. This is a simplifying assumption that is not generally realized as the lattice strain drives morphological transitions. Bulk diffusion is neglected, but in the exchanged layer, diffusion is presumed to be fast enough not to interfere with the exchange process. Assuming no deposition or sublimation, and neglecting the background pressures, mass conservation requires that

$$J_0 - J_{B2} = J_{A2} \tag{1}$$

The anion exchange is described as an interfacial reaction,

$$\text{III-}V_A(s) + 1/2\ V_{B2}(g) \rightarrow \text{III-}V_B(s) + 1/2V_{A2}(g) \tag{2}$$

The ‘s’ and ‘g’ in parentheses stand for solid and gas, respectively. The equilibrium constant, K, for this reaction can be shown to be

$$K = K_{III\text{-}VA}/K_{III\text{-}VB} \tag{3}$$

where $K_{III\text{-}VA}$ and $K_{III\text{-}VB}$ are equilibrium constants for sublimation

$$\text{III-V}(s) \leftrightarrow \text{III}(g) + 1/2V_2(g) \tag{4}$$

Listed in Table 2.1 are the equilibrium constants for the III-V compounds, which are calculated based on thermodynamic data [6], except those for As_2. As pointed by Hurle [7], the standard heat of formation of As_2 molecules (ΔH^0_{298} ~ 53.5 kcal/mole) is too large. We, therefore, use the data provided by Pupp [8]. For As_2, the formation heat is 44.4 kcal/mol, and 34.4 kcal/mol for As_4. The equilibrium constant for $As_2 \leftrightarrow As_4$ is also included in Table 2.1. We will use this value in the discussion of the effect of As_4 on the exchange reaction.

Table 2.1: Equilibrium constants for sublimation of III-V Compounds and the maximum sublimation temperature (T_{sub1}) and the temperature of non-congruent dissociation (T_{sub2})

Reaction	$K_{III-V}=P_{III}P_V^{1/2}$ (kT in eV)	T_{sub1} (°C)	T_{sub2} (°C)
$Al_{(g)}+1/2P_{2(g)} \leftrightarrow AlP_{(s)}$	$3.86\times10^{11}\exp(-5.84/kT)$		
$Al_{(g)}+1/2As_{2(g)} \leftrightarrow AlAs_{(s)}$	$5.00\times10^{11}\exp(-5.58/kT)$	902	974
$Al_{(g)}+1/2Sb_{2(g)} \leftrightarrow AlSb_{(s)}$	$2.79\times10^{11}\exp(-5.10/kT)$		
$Ga_{(g)}+1/2P_{2(g)} \leftrightarrow GaP_{(s)}$	$4.19\times10^{11}\exp(-4.58/kT)$	571	774
$Ga_{(g)}+1/2As_{2(g)} \leftrightarrow GaAs_{(s)}$	$5.44\times10^{11}\exp(-4.55/kT)$	630	723
$Ga_{(g)}+1/2Sb_{2(g)} \leftrightarrow GaSb_{(s)}$	$2.71\times10^{12}\exp(-4.53/kT)$		
$In_{(g)}+1/2P_{2(g)} \leftrightarrow InP_{(s)}$	$1.66\times10^{11}\exp(-4.14/kT)$	268	684
$In_{(g)}+1/2As_{2(g)} \leftrightarrow InAs_{(s)}$	$2.05\times10^{11}\exp(-4.09/kT)$	508	688
$In_{(g)}+1/2Sb_{2(g)} \leftrightarrow InSb_{(s)}$	$4.37\times10^{10}\exp(-3.97/kT)$		
$Ga_{(g)}+1/4Sb_{4(g)} \leftrightarrow GaSb_{(s)}$	$2.73\times10^{10}\exp(-3.88/kT)$		
$In_{(g)}+1/4Sb_{4(g)} \leftrightarrow InSb_{(s)}$	$4.39\times10^{8}\exp(-3.32/kT)$		
$As_{2(g)} \leftrightarrow 1/2As_{4(s)}$	$5.00\times10^{-5}\exp(1.18/kT)$		

The product III-V_B mixes with III-V_A and forms a III-$V_{A\,(1-x)}V_{Bx}$ solid solution. This process is spontaneous for all the III-V compound semiconductor alloys in the MBE temperature range, although the solution may be metastable, as is the case for Ga-$As_{(1-x)}Sb_x$ ternary alloys. Based on a regular solution model [9], the activities of the components in the solution, denoted by [III-V] take the form:

$$[\text{III-V}_A] = x \exp[\Omega(1 - x)^2/kT] \quad (5)$$

$$[\text{III-V}_B] = (1 - x) \exp[\Omega x^2/kT] \quad (6)$$

where the interaction energy Ω and kT are measured in electron volts (eV).

Let ρ_s represent the atomic density on the surface and N represent the number of monolayers participating the exchange reaction, the total number, N_t, of V_A atoms being replaced by V_B is

$$N_t = xN\rho_s = xNs = 2J_{A2} \quad (7)$$

By combining Eqs. (1), (7), we get

$$Q = \frac{x}{1-x}\exp[\frac{\Omega}{kT}(1-2x)]\left(\frac{m_{A2}}{m_{B2}}\right)^{0.2.5}\left(\frac{2J_0}{N_s x}-1\right)^{-0.5} \quad (8)$$

where m_{A2} and m_{B2} are the molecular weights of V_{A2} and V_{B2}. When the reaction reaches its equilibrium, Q = K, the molar fraction of exchange, x, is determined. In this equation, the exponential term measures how far the solid solution deviates from an ideal solution.

The number of monolayers, N, in the exchange reaction is unknown. In our calculation, we use the ratio J_0/N_s as an input. One can readily incorporate the thickness of the exchanged layer into our results. However, for the sake of clarity and simplicity (to compare different reactions), our discussion assumes one monolayer exchange and the exposed surface is (001). In this case, for BEP = 10^{-6} Torr, J_0/N_s is about 0.2 ($\rho_s \sim 5.5 \times 10^{14}/cm^2$).

We consider P-for-As (strong-for-weak) and Sb-for-As (weak-for-strong) as examples to illustrate the thermodynamic characteristics of the exchange reactions. As will be shown below, the equilibrium constants for the exchange reactions are weakly temperature-dependent. The impact of temperature is much less remarkable than other factors, such as J_o. In our examples, we have tried to use the same temperatures as experimentally used.

2.1.2. P/As Exchange

Strong-for-weak bond exchange is expected to occur under normal exposure experimental conditions. This is what we obtain from thermodynamic prediction, as shown in Fig. 2.1.2 (a) and (b), where the exposed surfaces are GaAs (001) and InAs (001), respectively.

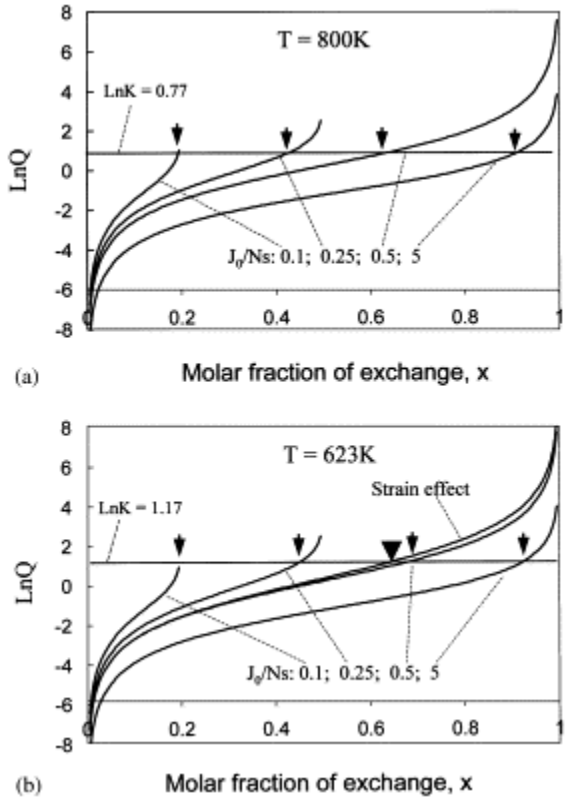

Figure 2.1.2: Exposure to P_2. (a) GaAs (001) exposed to P_2 and (b) InAs (001) exposed to P_2.

The arrowheads indicate the exchanged molar fraction at equilibrium. The exchange reactions and their equilibrium constants for these two cases are:

$$GaAs(s) + 1/2\ P_2(g) \rightarrow GaP(s) + 1/2As_2(g),\ K = 1.30\ \exp(0.035/kT) \qquad (9)$$

$$InAs(s) + 1/2\ P_2(g) \rightarrow InP(s) + 1/2As_2(g),\quad K = 1.23\ \exp(0.052/kT) \qquad (10)$$

It can be seen that the exchanged molar fraction, x, of GaP or InP increases with the ratio of J_o/N_s. Under small fluxes ($J_o/N_s < \sim 0.25$), almost all the incoming P_2 molecules are exchanged. When the flux increases to $0.5N_s$, which corresponds to a BEP of about 1.6×10^{-6} Torr (assuming one monolayer exchange), about 60% of the As atoms in an InAs (001) monolayer are replaced by P atoms. It can also be seen that the degree of exchange increases with the increase in bond strength difference.

It should be noted that the backward reaction represents As-for-P (weak-for-strong) exchange. Therefore, under the same J_o/N_s condition, the As-for-P exchange can hardly occur for small J_o/N_s. To get appreciable exchange, the J_o/N_s should be larger than $\sim 1 \times 10^{-6}$ Torr.

2.1.3. Sb/As Exchange

In Fig. 2.1.3, the variation of the reaction quotients with molar fraction, x, of exchange under different J_o/N_s conditions is shown.

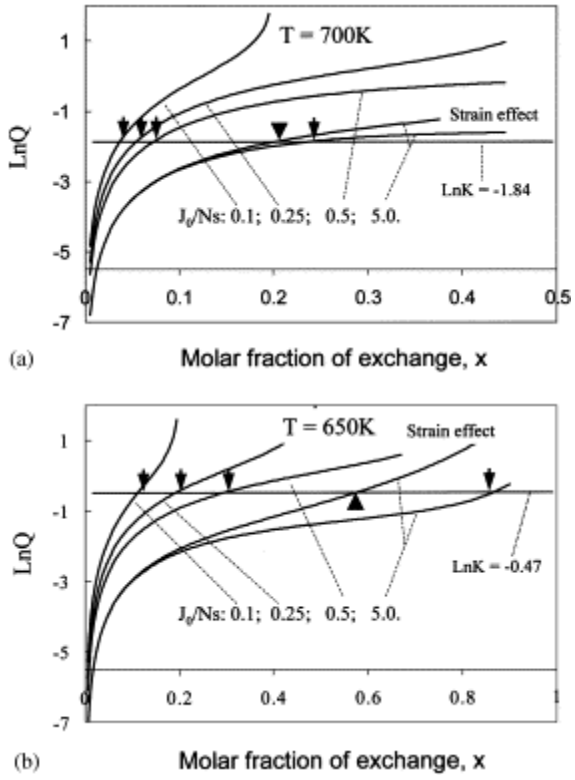

Figure 2.1.3: Sb_2 Exposure. (a) GaAs (001) exposed to Sb_2 and (b) InAs (001) exposed to Sb_2.

The exposed surfaces are GaAs (001) and InAs (001). The exchange reactions and equilibrium constants, respectively, are:

$$GaAs(s) + 1/2\ Sb_2(g) \rightarrow GaSb(s) + 1/2As_2(g),\ K = 0.20\ \exp(-0.02/kT) \qquad (11)$$

$$InAs(s) + 1/2\ Sb_2(g) \rightarrow InSb(s) + 1/2As_2(g), \quad K = 4.69\ exp(-0.12/kT) \qquad (12)$$

As expected, the weak-for-strong-bond exchange is very small. For example, under J_o/N_s = 0.25, which corresponds to a BEP of 1.6×10^{-6} Torr, x = 0.05 for GaAs (001). In contrast, almost all As_2 molecules are exchanged for the As-for-Sb reactions under the same conditions, qualitatively in agreement with the experimental observations.

In reality, there are a number of factors that may have large impact on the thermodynamic equilibrium. They may not be able to reverse the reaction directions, but they are indeed able to shift the equilibrium point. These factors are discussed in detail below.

2.1.4. Bond Strength

Although the exchange reaction is often discussed in terms of bond strength, the direction of exchange reaction is determined by the total free energy change, rather than by bond strength. However, under normal MBE conditions, bond strength can be used as a first guide for determining the tendency of exchange. Fig.2.4 shows the equilibrium constants in the MBE temperature range for some typical exchange reactions. Note the weak temperature dependence of the equilibrium constants. It can be seen that the larger differences in bond strength have larger equilibrium constants for strong-for-weak-bond exchange (or smaller K for weak-for-strong-bond exchange), implying larger degree of exchange.

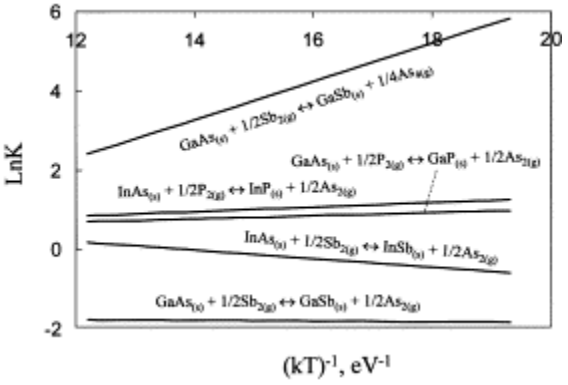

Figure 2.4: Equilibrium constant. Temperature dependence of equilibrium constant for some typical exchange reactions

2.1.5. Mixing Interaction Energy

When foreign or solute atoms are put into a host lattice, lattice distortion is produced corresponding to the atomic size difference. The amount of strain energy, related to the lattice

distortion, and also the chemical potential of the constituent components, is measured in terms of the mixing interaction energy. The effect of the interaction on the equilibrium of the exchange reaction is reflected by the term exp[(1-2x) Ω/kT)]. The interaction energy, Ω, which is related to the regular solution model, has been shown to be directly proportional to the square of lattice mismatch. Based on the delta-lattice-parameter model proposed by Stringfellow [10], Ω is 147.5 meV for Ga-As-Sb, 98.5 meV for In-As-Sb, 42.5 meV for Ga-As-P, and 25.2 meV for the In-As-P system. Consequently, the greatest effect of the interaction energy is expected in the Ga-As-Sb ternary alloys. The equilibrium point is shifted in the lower x direction when $x < 0.5$ (usually for weak-for-strong-bond exchange), and for $x > 0.5$, to the higher x direction. Interpretation of this effect is simple. When $x < 0.5$, the lattice distortion energy increases with addition of solute V_B atoms to the host III-V_A lattice. This energy increase process automatically results in shifting of the equilibrium point to smaller x. For $x > 0.5$, the host lattice is converted from III-V_A to III-V_B. Increasing x is equivalent to decreasing the solute (now V_A) concentration, and hence the equilibrium is shifted to higher x values. A quantitative comparison is shown in Fig. 2.1.5. It can be seen that remarkable effects can be expected when the equilibrium x is away from 0.5.

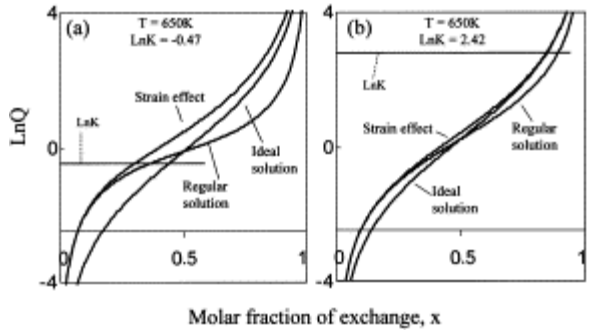

Figure 2.1.5: Surface Exposure to Sb_2 and P_2. (a) InAs (001) exposed to Sb_2; (b) GaAs (001) exposed to P_2.

2.1.6. Strain Energy

As a result of atomic differences, the lattice constant of the solid solution III-$V_{A(1-x)}V_{Bx}$ is different from that of the substrate III-V_A, giving rise to lattice mismatch. Consequently, the surface layer is strained and elastic strain energy is built up during the anion exchange, thereby increasing the chemical potential of the constituent components. The amount of strain energy stored depends on the molar fraction, x. Assuming the lattice constants obey Vegard's law and no plastic relaxation occurs, the strain energy E_{Str} (in eV) takes the form of

$$E_{Str} = 1.037 \times 10^{-11} \frac{m_i}{\rho}\left(C_{11} + C_{12} - \frac{2C_{12}^2}{C_{11}}\right)\varepsilon_0^2 x^2 \text{, in eV} \qquad (13)$$

where m_i is atomic weight, ρ the density (g/cm^3); the C's are elastic constants (Pa), ε_0 the misfit strain when x = 1.

As expected, the stored strain energy in the exchanged surface layer always shifts the equilibrium point to lower molar fractions. In other words, the strain effect always resists the exchange process on a strain-free flat surface. This is in contrast with the case where anion exchange reduces strain for an initial three-dimensional (or islanded) surface. In this case, the strain energy in the system maybe reduced by the anion exchange, thereby providing a driving force for size reduction of three-dimensional islands, or flattening of the surface.

The effect of strain energy on the equilibrium is shown in Fig. 5, where the contributions of non-ideality of the solid solution and strain effect are compared with respect to the ideal solution. More comparisons are shown in Figs. 2.1.2, 2.1.3, and 2.1.6.

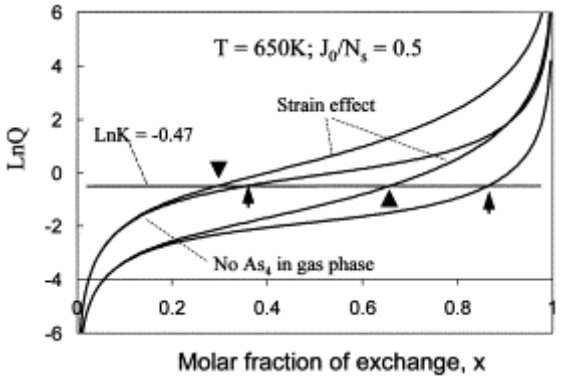

Figure 2.1.6: InAs (001) exposed to Sb_2.

For group-V species, an equilibrium, exist between tetrameric and dimeric form:

$$V_2(g) \leftrightarrow 1/2V_4(g),\ K_{V4} = P_{V4}^{1/2} P_{V2}^{-1} \qquad (14)$$

Depending on the exchange temperature, this equilibrium can have drastic impact on the exchange reaction. Within the temperature range of 530-730 °C, P_2 is the dominant phosphorus species over InP. Only up to 10% of the total phosphorus flux consists of P tetramers [11,12]. Fluxes originating from the (001) InP surface heated in the UHV between 330-420°C consist

of only P dimers [11]. These results indicate that in the practical exchange temperatures, the involvement of P tetramers can be neglected.

For $Sb_2(g) \leftrightarrow 1/2Sb_4(g)$, it is predicted that the dominant equilibrium antimony species is the Sb tetramer below 530°C, based on the thermodynamic data [13]. Under a total pressure in the range of 10^{-7} - 5×10^{-6} Torr, about 90% of the molecules are Sb_4. Therefore, Sb_4 molecules are expected to dominate in the flux from the surface at typical MBE conditions.

For $As_2(g) \leftrightarrow 1/2As_4(g)$, experimental results indicate that below 350°C, the tetrameric As_4 dominates in the flux from a heated GaAs surface, irrespective of the type of arsenic molecules impinging on the surface. At temperatures of 450°C and higher, dimeric arsenic molecules take over in dominance [14,15]. These results essentially agree with the thermodynamic predictions [16,17].

$$Q = \frac{x}{1-x}\exp[\frac{\Omega}{kT}(1-2x)]\left(\frac{4m_{A2}}{m_{B2}}\right)^{0.2.5}\left(\frac{\sqrt{1+AN_s x}-1}{A(2J_o - xN_s}\right)^{0.5} \qquad (15)$$

where

$$A = \frac{4K_{V4}^2}{\sqrt{2}}\frac{P_0}{J_0}\left(\frac{m_{A2}}{m_{B2}}\right)^{0.5} \qquad (16)$$

Fig. 2.1.6 shows the effect of As_4 involvement in the exchange reaction when InAs is exposed to Sb_2. For convenience of comparison, the no-As_4-involement data is also duplicated form Fig. 2.1.3a. It can be seen that the effect of As_4 on the equilibrium is remarkable. The molar fraction x increases from 0.30 to 0.66 under the same exposing conditions. From Fig. 2.1.4, it can also been seen that the equilibrium constant is very strongly temperature dependent.

2.1.7. Surface Structure and Surface energy

Of all the factors influencing the reaction thermodynamics and kinetics, surface structure and surface energy may be the most important. Semiconductors have reconstructed surface structures in order to assume a lower energy state under MBE conditions. Therefore, the surfaces may have considerably different thermodynamic properties from their bulk state. As a result, the equilibrium state that is predicted based on the bulk material properties may be far away from the actual one. Unfortunately, few thermodynamic data are available for any quantitative discussion. Intuitively, the shifting of the equilibrium point is expected to be more significant for the case where anion exchange results in a transition in surface reconstruction (e. g. (1 × 3) GaSb to (2 × 4) GaAs) than the case where no surface structure transition is involved.

Anion exchange mostly occurs in the first one or two monolayers. Other reactions lead to much more broadened interfaces. Therefore, the surface energy occupies a large portion in the total energy involved in the exchange process. Even a small change in the surface energy may give rise to a large shift in the equilibrium state. However, due to the lack of surface energy data, we can only make some qualitative assertions. Consider the As-terminated (001) surface energy. It is reported that this surface energy is 2100 meV per nm^2 [18]. So for each As atom, surface energy is about 335 meV, up to ten times higher than the misfit strain energy. For weak-for-strong-bond exchange (e.g. Sb-for-As), the surface energy will be reduced because of the formation of weak bonds on the surface, and hence, the exchange reaction will be favored energetically. In contrast, strong-for-weak-bond exchange will tend to increase the surface energy, and hence, will be reduced by the change in surface energy.

2.1.8. Segregation

In our model, the exchanged molecules are presumed to depart the surface after exchange. This is not always true. Segregation can occur in some material systems. Although this is a post-exchange process, it can have large impact on the equilibrium point. The most problematic anion is antimony (Sb). It has been reported that, in the heteroepitaxy of InAs/GaInSb structures, the InAs-on-GaInSb interfaces are tens of monolayers thick. The presence of Sb on the growing surface can be detected even at an InAs layer thickness of 200 nm [19]. Much more convincing results are reported recently by Kaspi [20], who used desorption mass spectrometry to monitor the chemistry of the flux departing the surface *in-situ*. The segregated Sb is incorporated into the lattice of the InAs, forming a broad, strained and Sb-graded interface.

2.2. Chemical Models for Sb/As, As/Sb, and P/As Heterostructures

We show in this section that their significant complexity in the anion exchange and interdiffusion process. In comparison to the previous section, we see that surface structure and anion interactions are key to our experimental observations. Revisiting of the analysis in Section 4.1 is advisable from these results.

The exposure of GaAs and GaSb surfaces to P, As, and Sb beams was carried out to understand the extent of and driving forces for anion exchange during structure formation. Numerous factors were compared. These include: substrate temperature, surface preparation (reconstruction), anion flux species (dimer or tetramer) and exposure time. Superlattice structures are prepared not through direct growth, but by the exposure of the semiconductor surface to a different anion flux at a specific temperature and for a specific time (same type of structure analyzed theoretically in Section 2.1 of this report). Through the analysis of data derived from a range of characterization techniques, including RHEED, high resolution x-ray diffraction (XRD), spectroscopic ellipsometry (SE), and AFM, we have created models of the structures and inferred primary driving forces for creating the observed structures. Chemical models are then articulated which capture the reactions present during junction synthesis.

In our studies, As/Sb and Sb/As anion exchange reactions were investigated by exposure of

GaSb surfaces to As_2 and As_4 species, and by exposure of GaAs to Sb_2, respectively. It is found that when GaSb surfaces are exposed to As, competitive reactions occur. These reactions are complex and indicate why a thermodynamic analysis, while important as "setting the stage" for understanding exchange, do not accurately predict experimentally-observed heterojunction characteristics. As shown herein, As exchanges with Sb in the GaSb resulting in the formation of GaAs bonds, and also reacts with Sb to form $AsSb_y$ isoelectronic compounds. The relative degrees to which GaAs and $AsSb_y$ are formed depend on the temperature, As exposure time, and the As species (i.e., As_2 or As_4) incident on the surface. It is found that As_2 is more likely to exchange with Sb in comparison to As_4, inhibiting the formation of $AsSb_y$. $AsSb_y$ interface segregation inhibits continued exchange. A specific As_4 exposure time and temperature exists wherein the formation of $AsSb_y$ is minimized. As_4 and As_2 have been previously observed to react differently on GaSb surfaces [19]. We also observe that As_4 is less reactive than As_2, and consequently As incorporation into GaSb layers is reduced when As_4 impinges on the GaSb surface. In the case of the Sb_2/GaAs system, Sb for As anion exchange does not occur to a significant degree, and surface segregation of Sb is found, with the subsequent incorporation of segregated Sb.

2.2.1 P/As: Impact of Temperature, Exposure Time, and Surface Reconstruction

As/P intermixing has also been studied for some time, particularly during the early exploration of the synthesis of GaInAs/InP by chemical beam epitaxy. Exposure of As-based compound surfaces to P is a standard procedure in beam switching sequences for the growth of a number of important heterostructures. When GaAs is exposed to P, the group V element may undergo P for As anion exchange, with the formation of a thin layer of GaP or GaP_yAs_{1-y}. Degradation of the interface quality has been found as a result of the interfacial segregation and exchange reaction between As and P. [21]

Both ($2x10^{-6}$ T) or high ($4x10^{-6}$ T) As_4 beam equivalent pressures were using during the synthesis of GaAs to prepare both As-lean and As-rich (relatively) GaAs surface reconstructions. It is found that the As-rich reconstruction reduces the phosphorus surface coverage and hinders P-for-As exchange. The effect of surface reconstruction on exchange and the functional dependences of P incorporation on temperature and exposure time indicate that P in-diffusion does not control the anion exchange. We introduce a reactive process that involves As on the GaAs surface. This process is the competitive formation of AsP compounds. In this framework, As on the surface is a sink for P, and thereby controls the extent of anion exchange. A chemical model including this competitive reaction and AsP isoelectronic by-product formation, in addition to P diffusion into the GaAs, is proposed. It can be seen that the competition between isoelectronic compound formation and exchange is a generalizable behavior across the materials systems we have investigated.

Twenty-period $GaAs_ySb_{1-y}$/GaSb (exposure of GaSb to As) and $GaSb_yAs_{1-y}$/GaAs (exposure of GaAs to Sb) structures were grown in a Varian Gen II MBE system equipped with valved cracker As and Sb sources. For the experiments in which GaSb was exposed to As, the structure was initiated with a GaSb buffer layer (~270Å) deposited onto a GaSb substrate. As_2 and As_4 fluxes were delivered to the Sb-stabilized GaSb surface for 10-30 s, over a substrate temperature range of 420 °C – 470 °C. The beam equivalent pressures (BEP) were As_4=$4x10^{-6}$

Torr, of As_2 =2x10^{-7} Torr (the BEP changes were a consequence of the variation in the cracker tip temperature, all other conditions were the same).

Ten-period $GaAs_yP_{1-y}$/GaAs (GaAs exposure to P) were synthesized in a Riber 2300 solid source MBE system with P and As valved cracker sources. During GaAs growth, two different As BEPs, 4x10^{-7} T and 2x10^{-6} T, were used to prepare different GaAs surfaces. RHEED measurements showed that the higher As flux yielded different variants of the (2x4) As-rich surface reconstruction, while the lower As flux results in an (2x1) GaAs surface reconstruction. The thickness of the GaAs layer was approximately 200Å. P incorporation in the structure was achieved by P_2 exposure (P_2 BEP = 4.5x10^{-6} Torr) of the GaAs surface and subsequent overgrowth of GaAs. The substrate temperature was varied from 420°C to 520°C, and the P_2 exposure time was varied from 10s to 50s.

For the Sb/As samples, angle-resolved XPS analysis was performed at take-off angles of 20°, 45° and 90°, corresponding to sampling depths of approximately 29, 61 and 87 Å, respectively. High-resolution spectra (pass energy = 17.90 eV) of the Ga 3d, As 3d, Sb 2d and Sb 3d photoelectron core levels were acquired. A spin-orbit splitting separation energy of 9.34 eV exists between the $Sb3d_{3/2}$ and $Sb3d_{5/2}$ levels. However, the Sb $3d_{5/2}$ peak suffers from interference with the O1s signal at the binding energy (BE) of 531 eV; hence, the Sb 2d core level was also considered, although the low splitting energy of 1.2 eV for the $Sb2d_{3/2}$ and $Sb2d_{5/2}$ renders the fit analysis difficult. In addition, care was taken since the Ga 3d plasmon loss tail interferes with the Sb 2d peak. Therefore, bond configurations of Sb were established by analysis of both Sb $3d_{5/2}$ and the Sb2d signals. Charging effects were corrected using the C 1s photoelectron peak from surface contaminants at 285.0 eV. The near-surface composition was estimated from the peak areas of the high-resolution spectra and using atomic sensitivity factors provided by Perkin-Elmer. For the P/As samples, high -resolution spectra of the Ga 3d, As 3d, P 2p O 1s and C 1*s* photoelectron core levels were acquired with a pass energy of 19.75 eV. The position of all the above peaks was calibrated using C 1*s* with binding energy BE = 284.6 eV. Angle-resolved XPS measurements were performed as described for the Sb/As samples.

The layered structure pseudodielectric functions, $\langle\varepsilon\rangle = \langle\varepsilon_1\rangle + i\langle\varepsilon_2\rangle$, were measured in the 1.5 – 5.5 eV photon energy range with an energy resolution of 0.02 eV with a phase modulated spectroscopic ellipsometer (UVISEL-Jobin Yvon) at multiple angles of incidence in the range 55° - 80° for Sb/As structures. Correspondingly, for the P/As structures the 0.75–6 eV photon energy region with an interval of 0.02 eV was used. The spectra were analyzed using the Bruggemann effective medium approximation [22]. The experimental data were fitted by minimizing the squared differences between the measured and calculated ellipsometric quantities [23]. Layer thicknesses and constituent volume fractions were used as the fit variables. Layer compositions are evaluated through analysis of the amplitude and energy position of the E_0 and E_1 interband critical points (CPs). To obtain a quantitative and consistent analysis, modeling of both XRD and SE spectra (for the P/As structures only) has been performed employing a multilayer model of the epitaxial structure. Specifically, the measured pseudodielectric functions of the samples have been analyzed using a repetition (superlattice) model GaAs-substrate/$(GaAs/GaP_yAs_{1-y})_{10}$/GaAs-oxide (where 10 is the number of periods grown) to take into account the effect of the surface oxide. A linear grade approximation was

used to model the in-diffusion of phosphorus. The linear gradient provides good fits to both SE and XRD spectra, and it was verified that the use of an exponential diffusion gradient does not improve the goodness of fit of the XRD data.

The structures were also characterized by high-resolution X-ray diffraction (XRD) in order to derive their quality and structural parameters such as the thickness and composition of layers. XRD analysis was performed with a Philips MRD system using Cu Kα radiation to obtain (002) θ/2θ scans. The superlattice structures were simulated with the dynamical diffraction theory using the Bede RADS software.

Finally, all of the P/As and a selection of the As/Sb and Sb/As structures were measured using atomic force microscopy (AFM) and all were monitored during growth by RHEED.

2.2.2. Sb/As and As/Sb Reactions

Figure 2.2.1 compares the Ga 3d, Sb 2d, Sb $3d_{5/2}$ and As 3d photoelectron peaks acquired for GaSb and GaAs substrates, and for a GaSb surface exposed to As_2 and As_4 fluxes for 10s at 420 °C. In the Ga 3d signal of the reacted samples, the GaAs (BE = 19.2 eV) and GaSb (BE = 19.6 eV) fit components have not been resolved because of the close binding energy values, and have been included in the same peak at 19.5 eV, which, therefore, has a relatively large full width at half maximum (FWHM) of 1.3 eV. Because the analysis is *ex-situ*, the Ga_2O_3 fit component at 20.5 eV is also present. In the Sd 4d photoelectron spectra, the Sb_2O_3 and Sb_2O_5 contributions have also been included in the same fit because of the small difference in binding energies. The splitting energy between Sb $2d_{3/2}$ and $Sb2d_{5/2}$ has been fixed at 1.2 eV, while the energy separation between Sb in GaSb and Sb in Sb_2O_3 and Sb_2O_5 has been set at 2.5 ± 0.4 eV. In the As 3d spectra of the GaSb samples exposed to the arsenic flux, a high energy component appears in addition to that of GaAs and As-oxides. This high energy peak has been ascribed to the formation of isoelectronic compound, $AsSb_y$, during the As for Sb anion exchange reaction. The $AsSb_y$ fit component is very broad because it can include isoelectronic components of different stoichiometry. Specifically, As can react with Sb resulting in AsSb, As_2Sb_3, As_3Sb.

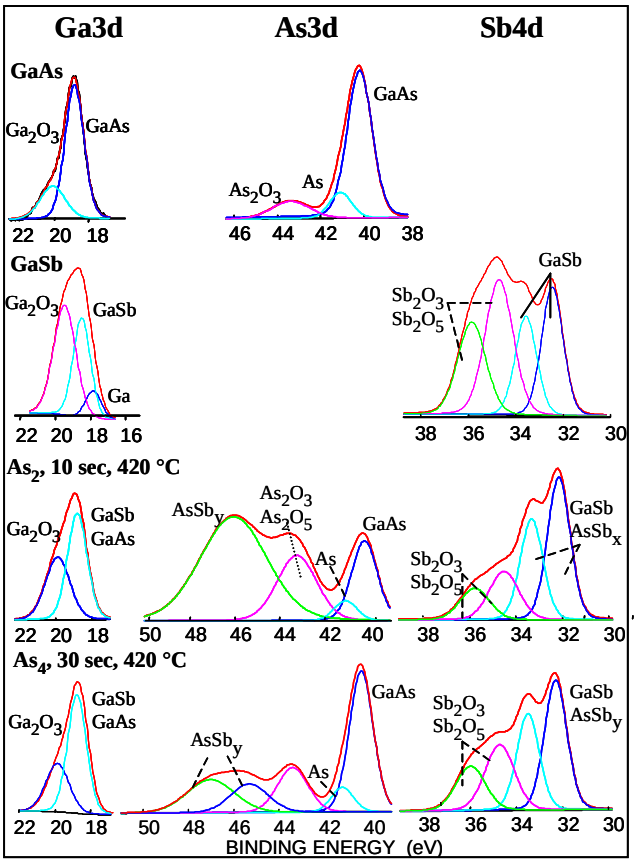

Figure 2.2.1: Photoelectron Peaks. Comparison of Ga3d, Sb2d, Sb3d5/2 and As4d high resolution photoelectron peaks for GaSb and GaAs substrates and for two typical GaSb layers exposed to As_2 at 10s and to As_4 at 30s and 420°C.

The high binding energy of $AsSb_y$ in the As_{3d} implies that, in the AsSby compound, the Sb is electronegative, and the As is electropositive. Consequently, the $AsSb_y$ contribution should be at low binding energy in the Sb2d photoelectron spectrum, and its binding energy value could be quite close to that of GaSb. This would be consistent with the increase of the ratio of the low binding energy peaks to the Sb oxide peak for samples with a corresponding high contribution of the $AsSb_y$ in the As3d peak. The angle resolved analysis of the GaSb layer exposed to the As_4 flux for 10s at 420°C is shown in Fig. 2.2.2, and shows that the intensity of the $AsSb_y$ component increases with take-off angle, i.e., the sampling depth, and become comparable to the GaAs component at high take-off angle, indicating that $AsSb_y$ segregates at the $GaAs_ySb_{1-y}$/GaSb interface.

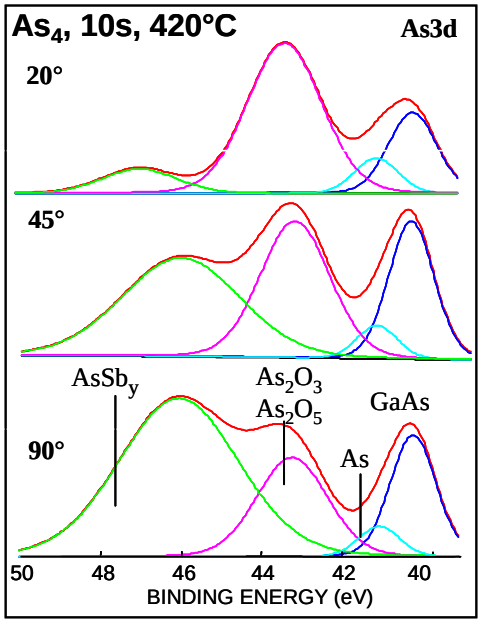

Figure 2.2.2: Angle-resolved As3d photoelectron peak recorded for a typical GaSb layer exposed to As_4 for 10s at 420°C.

The formation of GaAs bonds as a product of exchange and $AsSb_y$ formation depends on the incident As species, i.e., As_2 or As_4, on the As exposure time, and on the temperature. Fig. 2.2.3 shows the As 3d photoelectron spectra of GaSb layers exposed to As under different conditions. Under the present flux conditions, for an exposure time of 10s and a temperature of 400 °C, no appreciable GaAs is observed. The formation of GaAs on the surface exhibits a different temperature dependence, depending on whether As_4 or As_2 impinges on the surface. In particular, when As_2 impinges on the surface, the degree of exchange increases with temperature (independent of exposure time). In contrast, when As_4 is used, GaAs formation is maximized at 420°C. In addition, exchange increases as the exposure time increases. These different temperature dependences imply different reaction paths for anion exchange depending on the arsenic species.

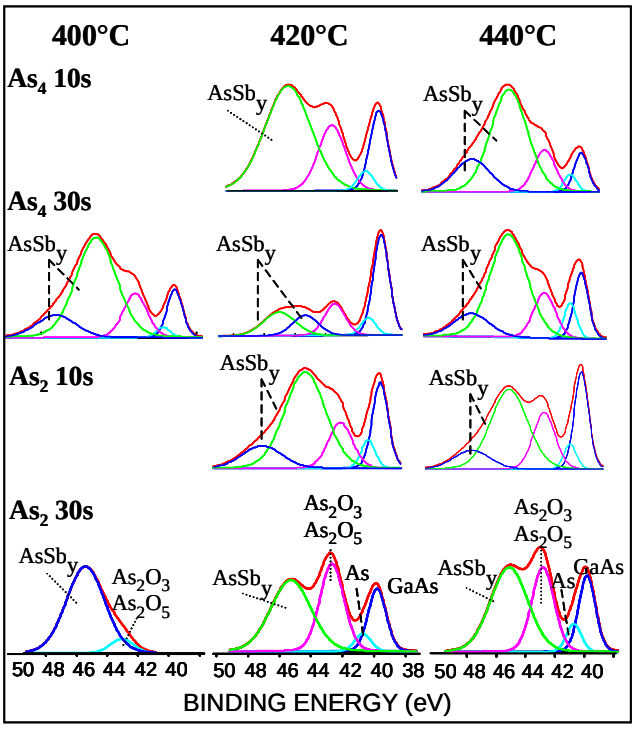

Figure 2.2.3: As3d photoelectron peaks acquired for GaSb layers exposed to As_2 and As_4 for different times and at different temperatures.

XPS does not show significant Sb-for-As exchange. The anion-to-Ga atomic percentage ratios are plotted for a GaAs layer after exposure to an Sb_2 flux for 100s at 550°C (Fig.2.2.4a) and for GaSb after exposure to an As_4 flux for 10s at 420°C (Fig. 2.2.4b). In both cases, it is found that the total anion-to-cation ratio, i.e., (Sb+As)/Ga, is higher than 1, indicating an excess of the anion component at the surface. Indeed, the difference between the two systems is that for the Sb-for-As anion exchange (Fig. 2.2.4a) the (Sb+As)/Ga decreases with the sampling depth, indicating that the anion segregates at the GaAs surface, while for the As-for-Sb anion exchange (Fig. 2.2.4b), the (Sb+As)/Ga ratio increases with sampling depth, indicating that the anion segregates at the $GaAs_ySb_{1-y}$/GaSb interface. Furthermore, Fig. 2.2.4a shows that it is the Sb/Ga ratio that increases at the outmost surface, providing evidence that Sb segregates at the GaAs surface. In contrast, Fig. 2.2.4b shows that while the Sb/Ga ratio decreases upon anion exchange, the As/Ga ratio increases with sampling depth indicating that some of the incorporated As is present at the inner interface in a form not bonded to Ga. Therefore, for the As for Sb exchange, the trends for the (As+Sb)/Ga and As/Ga ratios are consistent with the segregation at the inner interface of $AsSb_y$ compounds.

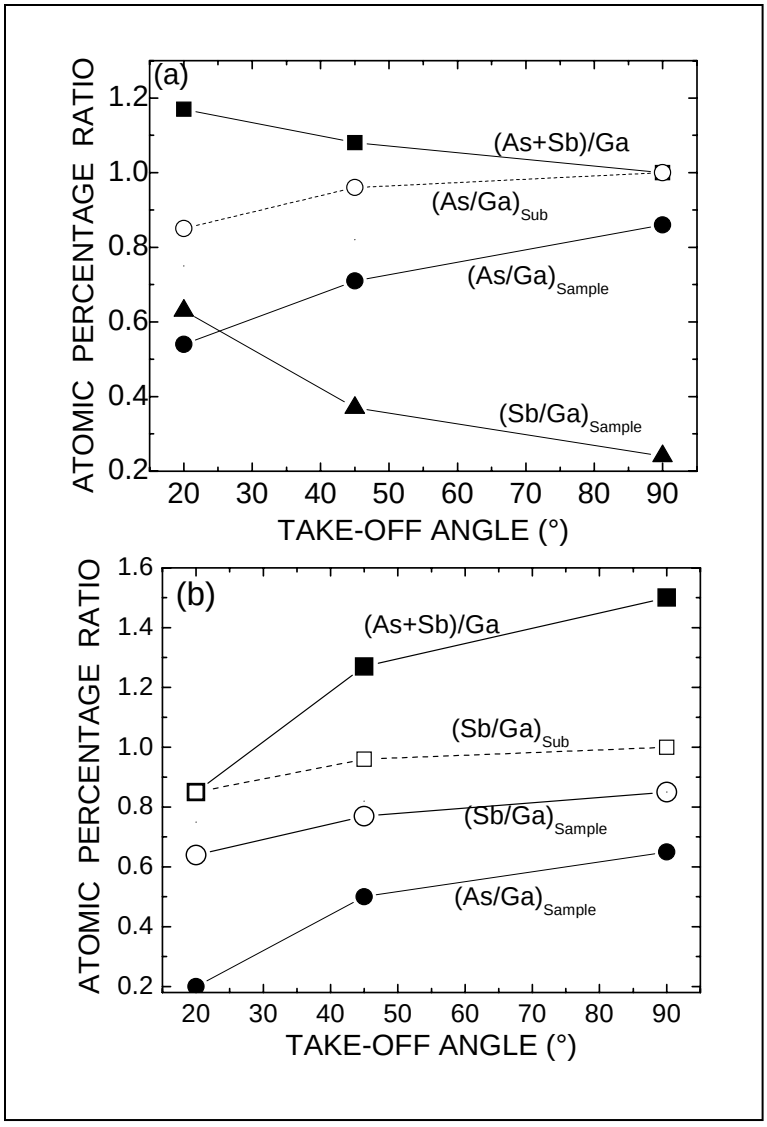

Figure 2.2.4: XPS quantitative ratios, as measured from the peak areas, (a) for a GaAs layer as grown and after exposure to Sb_2 for 100s at 550°C, and (b) for a GaSb layer as grown and after exposure to As_4 for 30s at 420°C.

The effects of temperature, As exposure time, and As species on the extent of the reactions for As/GaSb are summarized in Figure 2.2.5. It can be seen that in the case of As_2 exposure, no difference is found between the 10s and 30s exposure times, indicating that As_2 readily reacts, and exchange is not under kinetic/diffusion control under the present conditions. It is found that As_4 is less reactive than As_2, but more $AsSb_y$ is formed. However, this does not apply for all temperatures, and for As_4 exposure, a critical temperature of approximately 420°C exists were the anion exchange, i.e., GaAs formation, is favored at the expense of the $AsSb_y$.

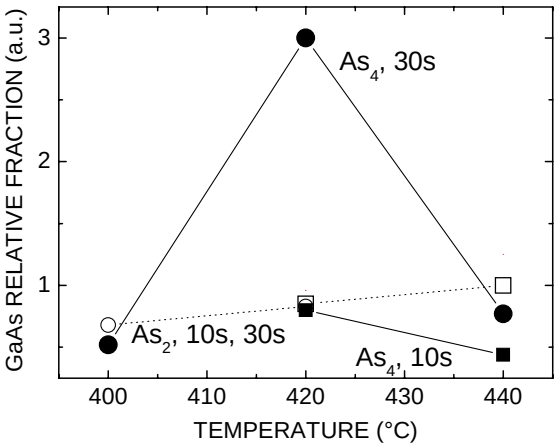

Figure 2.2.5: GaAs relative area as measured from the fit analysis of the As3d photoelectron peaks for GaSb layers exposed to As_2 and As_4 for 10s and 30s at various temperatures.

For the factors investigated in this study, the surface temperature has the most significant impact on surface morphology. Figure 2.2.6 shows AFM topographic images of GaAs layers exposed to Sb_2 for 100s at temperatures of 420 °C and 550 °C. It is seen that surface modification is enhanced as the temperature is increased. The Sb_2 exposure creates an oriented morphology, similar to that observed for AlGaAs surfaces exposed to indium [24]. For the case of As/Sb, the general trend is that surface roughness increases with temperature. However, a distinctly different morphology is observed at 420 °C, which corresponds to the temperature resulting in greater GaAs formation, and lower $AsSb_y$ formation as previously discussed. In comparison to the GaAs exposure to Sb, this surface shows no orientation effect.

Ellipsometric analysis of two samples obtained by exposing GaAs surfaces at 420 °C and 550 °C to Sb_2 for 100s are indistinguishable from that of a GaAs substrate with a native oxide surface layer. This indicates that significant Sb for As anion exchange does not occur. In order to increase the modeling accuracy, spectra were acquired at various angles of incidence from 55° to 80° for the 550°C sample, and were fitted simultaneously to a superlattice model $GaAs/(GaSb_yAs_{1-y}/GaAs)_{20}$/GaSb-oxide where fit variables were the layer thickness's and the exchanged layer composition.

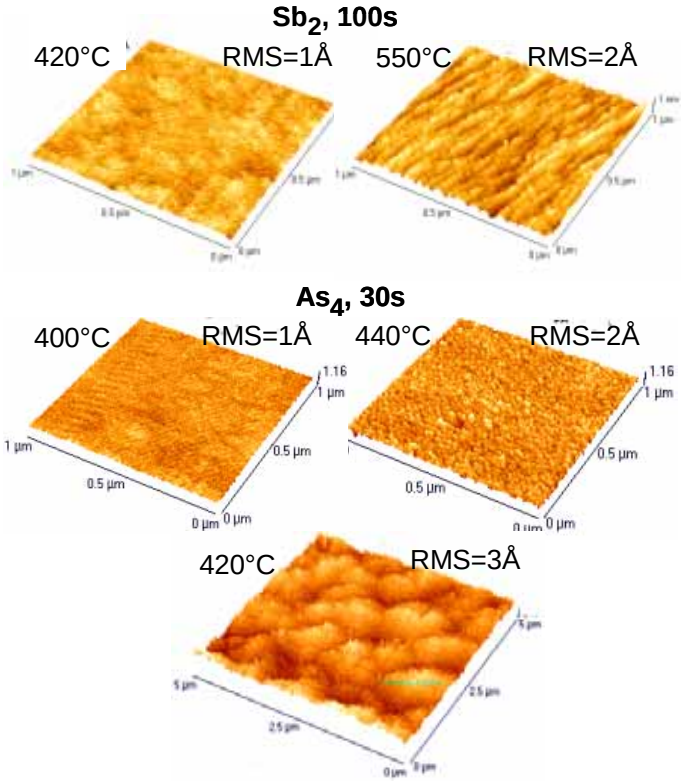

Figure 2.2.6: AFM 3D topographical images for GaAs layers exposed to Sb_2 for 100s at 420°C and 550°C, and for GaSb layers exposed to As4 for 30s at various temperatures. The surface roughness, rms, is also indicated. Lateral scale is 1μmx1μm for every image, but 5μmx5μm for last image

Figure 2.2.7 shows the best fit result of the variable angle spectra. These results indicate that when a GaAs layer is exposed to an Sb flux, the Sb does not diffuse into the GaAs but, instead, segregates at the surface. The Sb segregation at the GaAs surface is converted into GaSb and/or $GaSb_yAs_{1-y}$ when the Ga and As fluxes are initiated for the overgrowth of the subsequent GaAs layer. Furthermore, no diffusion of Sb into the overgrown GaAs layer is observed. Thus, an abrupt interface is achieved in $(GaSb_yAs_{1-y}/GaAs)_n$ structures formed by letting Sb_2 impinge on a GaAs epitaxial layer, as also confirmed by the intense and sharp interference fringes observed by XRD analysis of $(GaAs/GaSb_yAs_{1-y})_{20}$ structures published previously.

A similar approach has also been applied to the characterization of the As/Sb anion exchange and interface composition in $(GaSb/GaAs_ySb_{1-y})_{20}$ structures. Figure 2.2.8 shows a comparison among typical spectra of the real, $\langle\varepsilon_1\rangle$, and imaginary, $\langle\varepsilon_2\rangle$, parts of a GaSb substrate and the spectra recorded for two typical $(GaSb/GaAs_ySb_{1-y})_{20}$ structures obtained by exposure of the GaSb epitaxial layers to an As_4 flux for 10s and 30s at a temperature of 420 °C. The spectra of the structures differs from that of the GaSb substrate with native oxide, mainly in the region of

the E_1 and $E_1+\Delta_1$ interband critical points (CPs) that are strongly sensitive to material composition. In particular, for short As exposure time, an increase of the E_1 and $E_1+\Delta_1$ CPs amplitude is observed, while it decreases with respect to that of the GaSb substrate with native oxide for longer As exposure time. This indicates that the exchange occurs to a different extent depending on exposure time. A simple model assuming the formation of a ternary alloy does not fit the amplitude of the E_1 and $E_1+\Delta_1$ CPs.

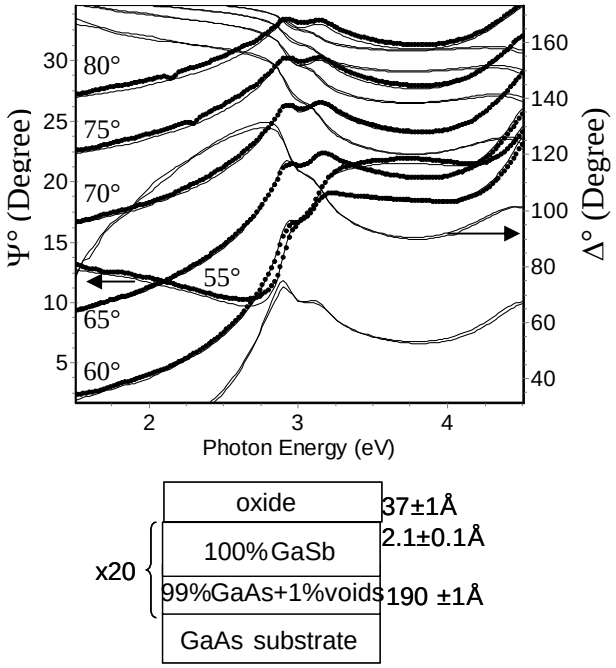

Figure 2.2.7: SE spectra acquired at various angles of incidence from 55° to 80° for a typical 20-period ($GaSb_yAs_{1-y}$)/GaAs obtained by GaAs layer exposure to an Sb_2 flux for 100s at 550 °C.

A good fit is obtained by a GaSb buffer layer thickness of about 270Å, and an exchanged layer with a total thickness of approximately 19 Å that includes a very thin interface layer containing some AsSb. The contribution of AsSb may be responsible for the increase of the E_1 and $E_1+\Delta_1$ CPs amplitude found for the sample exposed for 10s to arsenic. The dependence of the thickness of the exchanged layer and of the $AsSb_y$ segregation on the As species, temperature,

and As exposure time is summarized in Fig. 2.2.9. It is seen that the thickness of the exchanged layer is 15-16Å±1Å for an As exposure time of 10s and is 16-18Å±1Å for an As_2 exposure time of 30s. These data agree with the XPS data in Fig. 2.2.6, where a difference of 1-2 Å cannot be resolved. Furthermore, the thickness of the exchanged layer increases with temperature for As_2, while it has a maximum at 420 °C for As_4. The measured thickness dependence can be related to $AsSb_y$ formation and segregation at the GaAs/GaSb interface reported in Fig. 2.2.9b. In fact, the lower the $AsSb_y$ segregation, the greater the thickness of the exchanged layer, indicating that the $AsSb_y$ segregation inhibits anion exchange.

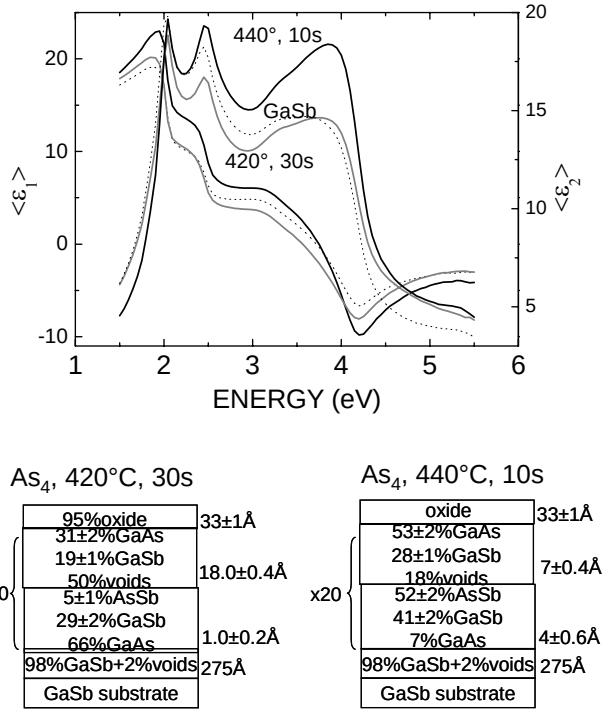

Figure 2.2.8: Typical spectra of the real, $<\varepsilon_1>$, and imaginary, $<\varepsilon_2>$, parts of a GaSb substrate and the SE spectra recorded for two $(GaSb/GaAs_ySb_{1-y})_{20}$ SLs obtained by exposure of the GaSb epitaxial layers to an As_4 flux for 10s and 30s at the temperature of 420°C.

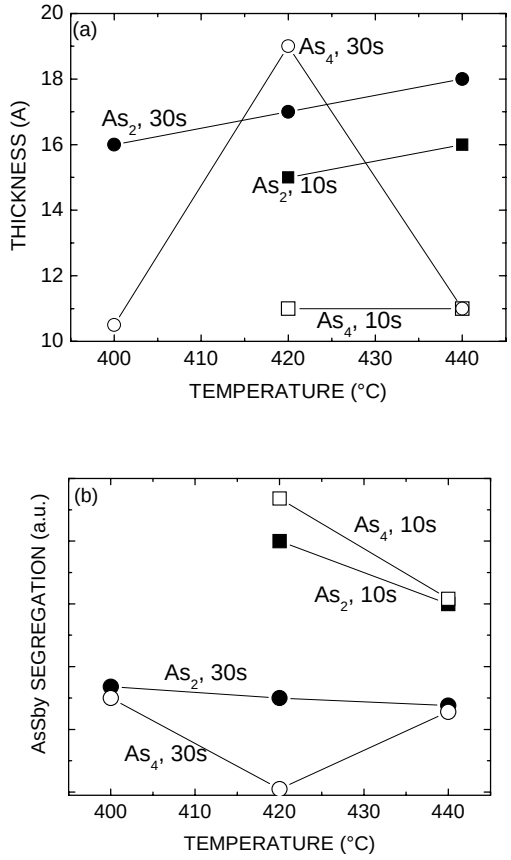

Figure 2.2.9: Temperature and time dependence of (a) the total exchanged layer and (b) $AsSb_y$ interface segregation as derived by SE analysis of ($GaSb/GaAs_ySb_{1-y}$)20 SLs obtained by As_2 and As_4 soak of GaSb layers.

4.2.3. P/As Reactions

The formation of Ga-P bonds, indicative of P-for-As exchange, is observed in the P 2p photoelectron spectra acquired for GaAs surfaces exposed to a P_2 flux at different temperatures and exposure times. Figure 2.2.10 shows the P/Ga ratio as calculated from the Ga 3d and P 2p peak areas for different temperatures and P exposure times It is found that the higher the temperature and exposure time, the larger the P surface coverage, which, however, is lower for the As-rich GaAs surface than for the As-lean surface. This indicates that more As on the GaAs surface hinders P surface coverage and exchange. At high temperature (520 °C) and long P exposure time, the two surfaces behave similarly because of the thermal desorption of the excess of As that acts as a surface barrier for the P uptake. The As-rich reconstruction of the GaAs surface reduces P incorporation, in agreement with previous work [25].

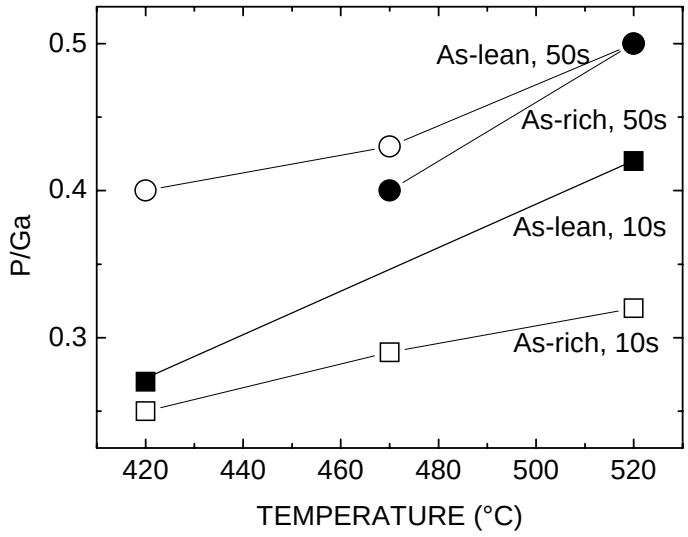

Figure 2.2.10: Surface P/Ga ratio derived from area ratio of the P2p and Ga3d XPS peaks for As-rich and As-lean GaAg layers exposed to P_2 at various temperatures for 10s and 30s. The XPS take-off angle is 20°.

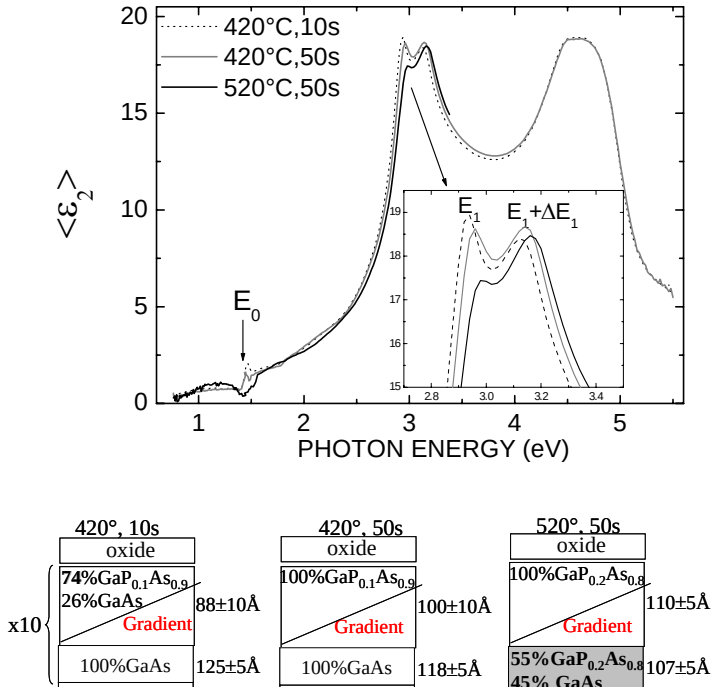

Figure 2.2.11: Spectra of the imaginary, $<\varepsilon_2>$, part of the pseudodielectric functions acquired for $(GaAs/GaP_yAs_{1-y})_{10}$ SLs by exposure of GaAs to a P flux at 420° for 10s and 50s and at 520°C for 50s. Inset: Detail of the E_1 and $E_1+\Delta E_1$ CPs. The corresponding best-fit models at bottom

Figure 2.2.11 shows typical ellipsometric spectra of the imaginary, $<\varepsilon_2>$, part of the pseudodielectric function of $(GaAs/GaP_yAs_{1-y})_{10}$ structures obtained by exposure of GaAs to a

P flux for different times and at different temperatures. The corresponding best fit BEMA models are also shown, as well as details of the E_0, E_1 and $E_1+\Delta E_1$ interband critical CPs. The details of E_1 and $E_1+\Delta E_1$ CPs (see inset) shows a blue-shift of the CPs and a gradual reduction with the increase of surface temperature and phosphorous exposure time. The dielectric function of GaP_yAs_{1-y} ternary alloys show a gradual evolution of the characteristic interband critical points with increasing phosphorous content from that of GaAs to that of GaP [26]. We derived the composition of the exchanged GaP_yAs_{1-y} layer, which ranges from y = 0.1 - 0.2 for the investigated temperature and phosphorous exposure time conditions. It is found that the GaP_yAs_{1-y} stoichiometry mainly depends on the GaAs surface reconstruction and on the temperature. In particular, for the As-rich GaAs surface reconstruction, a composition of 0.1 is found. In contrast, for the As-lean GaAs surface reconstruction, the phosphorous composition increases to 0.2. The thickness of the exchanged layer increases with phosphorus exposure time and temperature. In particular, the modeling analysis shows that for As-rich GaAs surface reconstruction and for T < 520 °C, P-for-As anion exchange occurs over approximately 100Å yielding a graded layer from the ternary $GaP_{0.1}As_{0.9}$ at the surface to GaAs. A GaAs layer approximately 100Å thick that does experience exchange is still present. In contrast, for the highest temperature of 520 °C and especially for the As-lean GaAs samples, P for As exchange and intermixing occurs over the entire 200Å GaAs epitaxial layer. The data for the exchanged layer are in good agreement with XRD analysis.

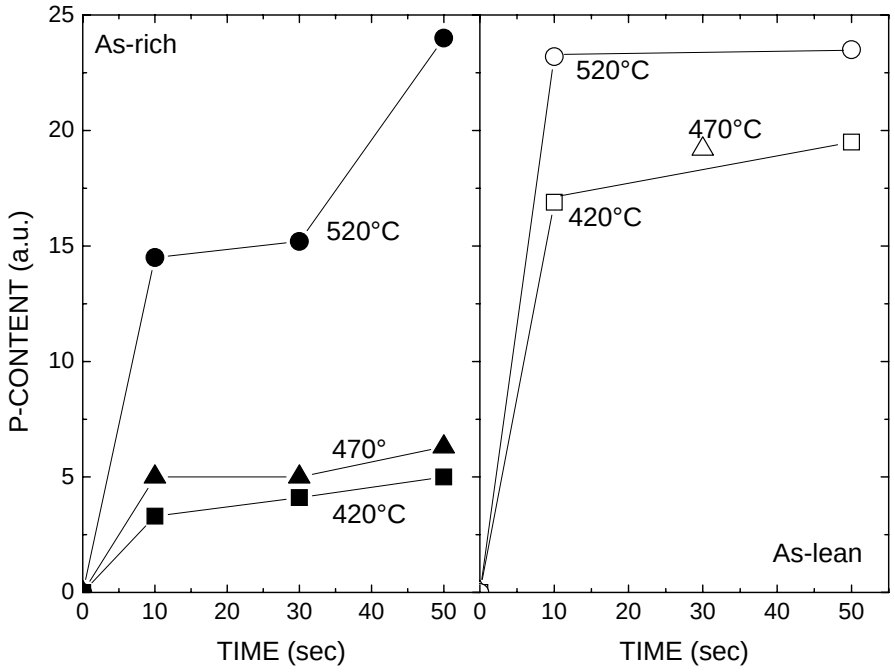

Figure 2.2.12: Dependence of integrated P content on P soak time, as estimated by analysis for As-rich (P_{As} = 4×10^{-6} Torr) and As-lean (P_{As} = 4×10^{-6} Torr) GaAs epitaxial layers exposed to the P_2 fluc at various temperatures.

The integrated phosphorus content has been calculated and reported in Fig. 2.2.12 as a function of phosphorus exposure time for various temperatures. It is found that the phosphorus content is higher for the As-lean GaAs epitaxial layer than for the As-rich GaAs, and in both cases

slightly increases with time ranging from 10s to 50s. The phosphorus content quickly increases in the first few seconds of exposure to phosphorus, indicating a very fast in-diffusion of P into GaAs. Therefore, anion exchange does not occur in the diffusion-controlled kinetic regime under the present conditions.

Figure 2.2.13 shows typical XRD rocking curves obtained from structures exposed to P_2 for 30 seconds and varying temp for: a) As rich surfaces, and b) As-lean surfaces. For lower temperature and exposure time and As-rich surfaces, the x-ray diffraction data indicate the formation of a well-ordered layers with many positive and negative superlattice peaks. The P composition is calculated from the separation of the 0^{th} order reflection and the substrate peak. The calculations assume that all of the strain is elastically accommodated - an assumption that is not equally accurate for all the samples, but provides an observation of trends in the data for comparison to SE and XPS. The dramatic difference in the phosphorus incorporation is clear in the comparison of the x-ray for the As-rich and lean surfaces. The absence of well-ordered negative peaks in Fig. 2.2.13b indicates the much greater incorporation of P in these structures and the greater degree of material strain and disordering. A comparison of x-ray data and the simulations used to fit the profiles are shown in Fig. 2.2.14. The profile simulated for SE and XRD are shown for comparison and indicate the high consistency obtained for the two different measurements and simulations. Finally, the predictions of a neural network process model that was derived from the XRD data are shown in Fig. 2.2.15. The surfaces show the dependence of P content on time and temperature and also show the measured variant of the (2×4) surface reconstruction for the ranges of growth conditions.

Surface topography was measured by atomic force microscopy (AFM). Fig. 2.2.16 shows the range of morphologies observed for the samples synthesized at: a) low temperature and exposure time and As-rich surface, and b) high temperature long exposure time and As-lean surface. At lower temperature, the morphology is characterized by the appearance of mounds which are typical of low temperature growth of GaAs. At high temperature the surface exhibits a cross-hatch morphology indicative of misfit dislocation formation and some degree of relaxation of the strain realized in the GaAsP layer. It is not clear if the strain and relaxation is uniform throughout the depth of the layer or gradually increases with the superlattice period.

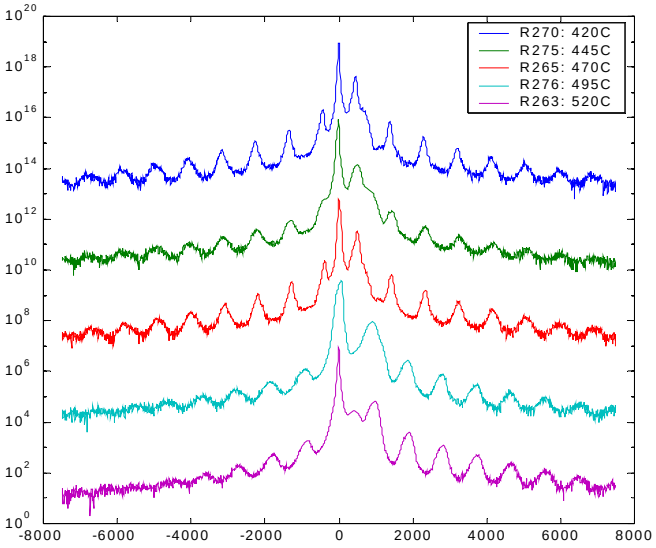

(a)

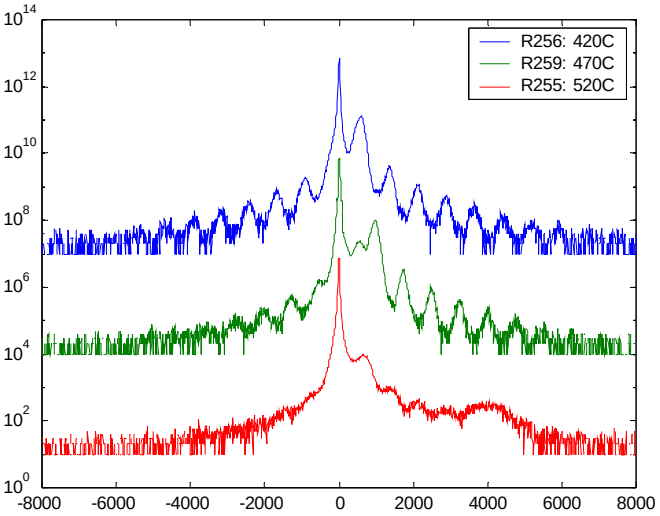

(b)

Figure 2.2.13: XRD data (004) for 30 sec P exposures for As-rich surface (a) and As-lean surfaces (b)

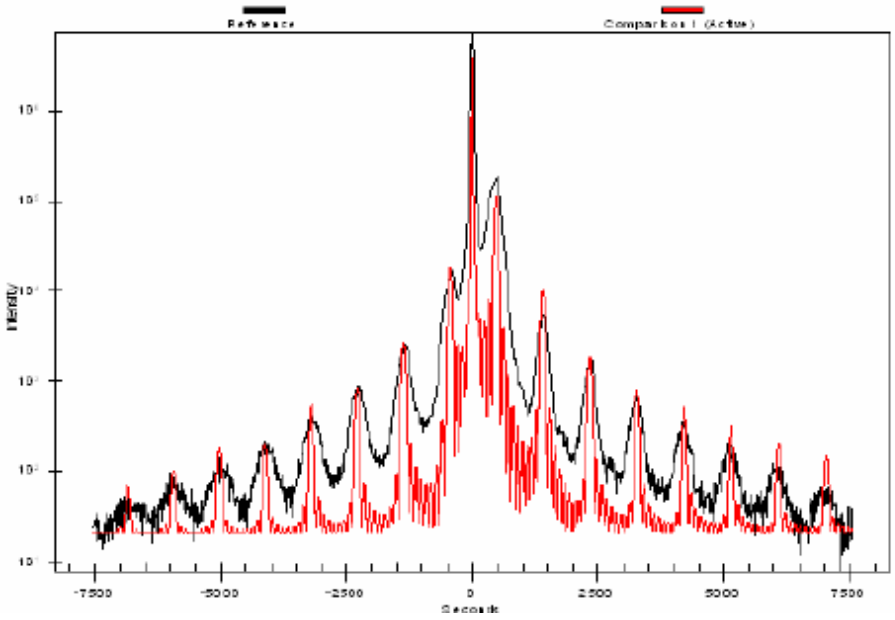

(a)

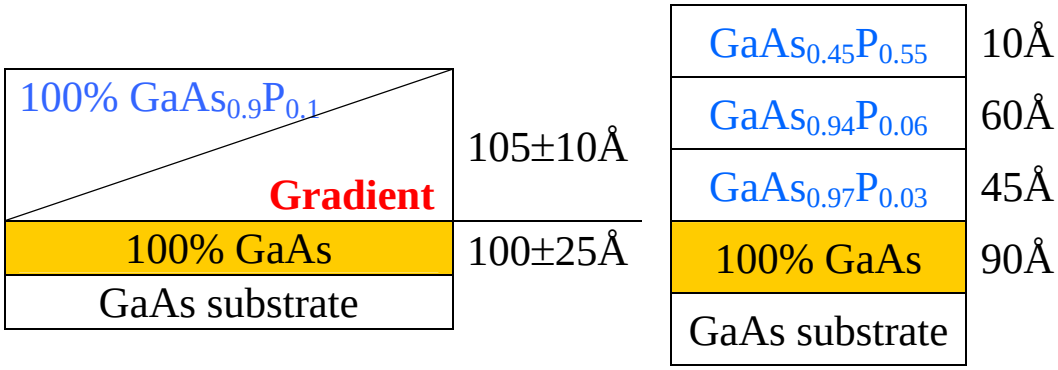

(b)

Figure 2.2.14: XRD data and fit with simulation for XRD (a) and SE (b) showing simulated structure comparison

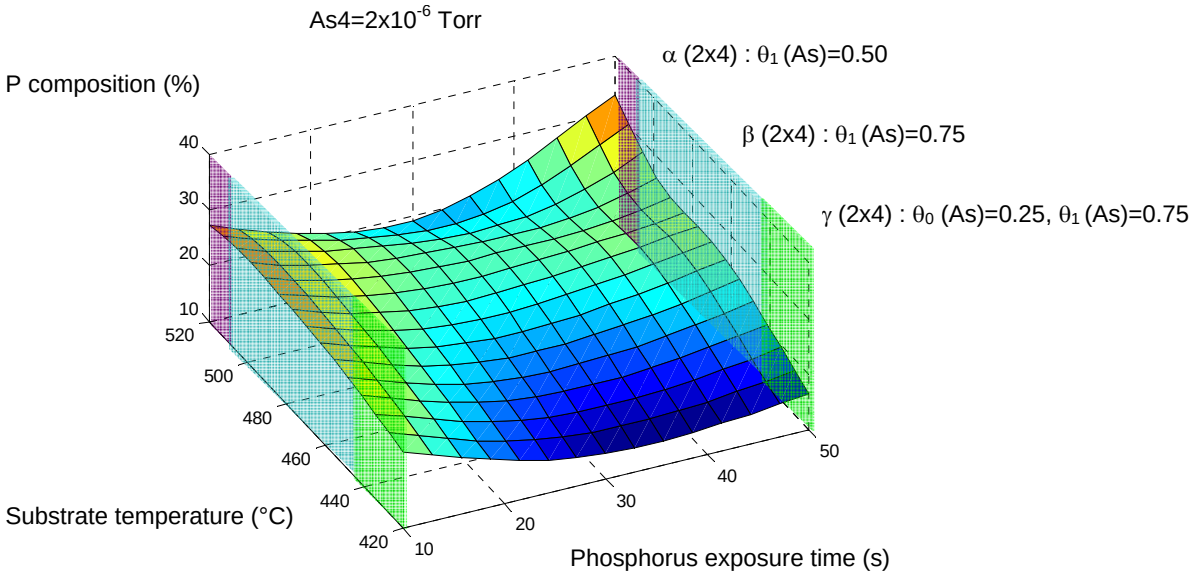

(a)

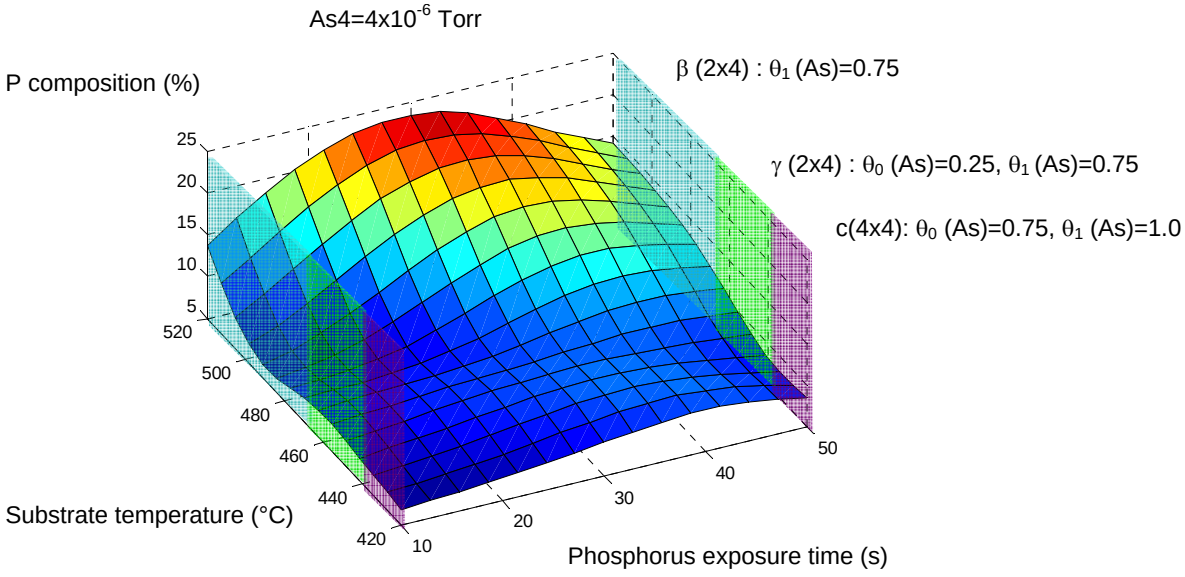

(b)

Figure 2.2.15: Neural network process models of P composition (from XRD analysis) as a function of temperature and exposure time for (a) As-lean and (b) As-rich surfaces. Variants of the (2×4) reconstruction are also shown

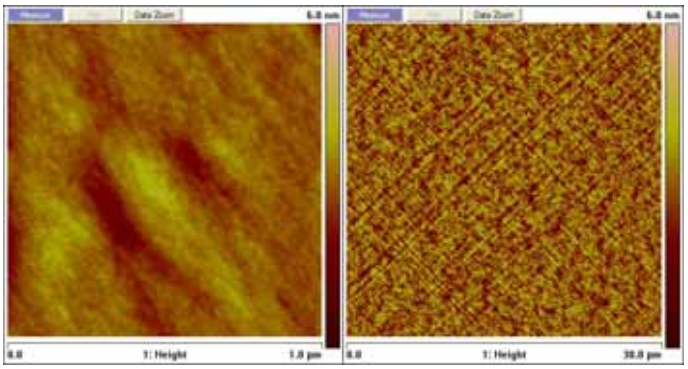

(a)

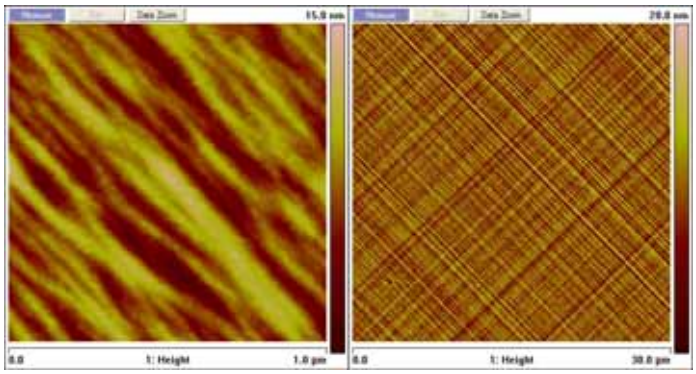

(b)

Figure 2.2.16: Topographic AFM iunages for P/GaAs (a) low temperature and exposure time and As-rich surface and (b) high temperature long exposure time and As-lean surface

4.2.4. Chemical Models for Sb/As, As/Sb, and P/As Surface Reactions

The Sb/GaAs is the most simple system examined and is characterized by Sb adsorption and subsequent incorporation. We therefore model it as:

$$\mathrm{Sb(g)} \underset{(1)}{\overset{K_{ads}}{\rightleftharpoons}} \mathrm{Sb(ads)} \xrightarrow[\substack{(2)\\ Very\ low}]{D} \mathrm{Sb(s)} + \mathrm{GaAs} \xrightarrow[(3)]{k_{exch}} no\ reaction \qquad (17)$$

where (1) is the surface chemisorption of antimony, (2) is the diffusion step and (3) is the reactive step with the corresponding rate constants.

Surface reactivity requires overcoming the energetic barrier for surface to bulk atomic in-diffusion ($E^{s\to b}$) and for bulk to surface exchanged anion out-diffusion ($E^{b\to s}$). For As on GaSb, the driving force $E_{As}^{s\to b} - E_{Sb}^{b\to s} > 0$ is because of the faster in-diffusion of As; however, the very low out-diffusion of Sb causes $AsSb_y$ to segregate at the GaAs/GaSb interface. Therefore, the in-diffusion of As is not rate limiting, and as demonstrated by the data presented

for As_2 which indicates that the exchange is not kinetically limited, we conclude that a simple diffusion-based model cannot explain the different products and reactivity observed for As_2 and As_4. For this reaction, the following steps should be considered: (1) chemisorption of the As on the GaSb surface; (2) in-diffusion of As through the GaSb layer and through the product $GaAs_ySb_{1-y}$ layer; (3-6) chemical reactions at the $GaAs/GaAs_ySb_{1-y}$ surface involving As for Sb exchange with the formation of GaAs and of the byproduct involving the exchanged Sb, i.e., $AsSb_y$; (7) outward diffusion of the Sb products and desorption or, as in the present case, interface segregation. Based on these assertions and the data, the chemical model for the interaction of As_2 and As_4 with GaSb can be described by:

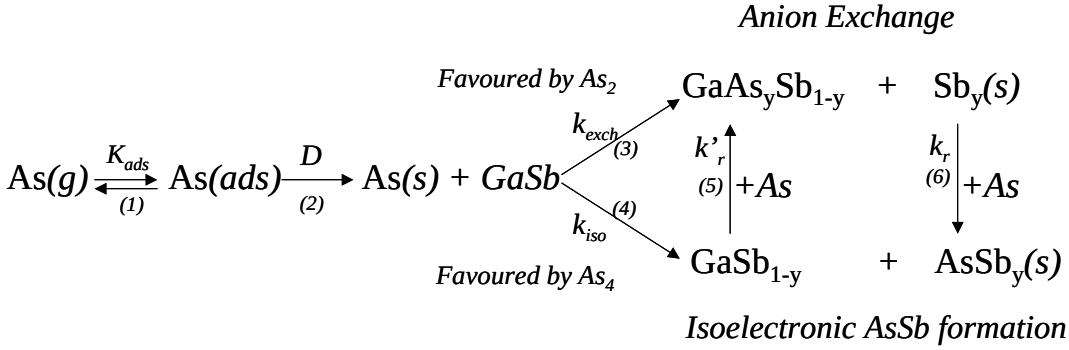

(18)

where K_{ads} is the chemsiorption constant, D is the diffusion coefficient for the indiffusion of As atoms, k_{exch} and k_{iso} are the true rate constants of the reactive step at the GaSb surface yielding anion exchange and isoelectronic formation, respectively, and k_r and k_r' are the rate constants for the recombination of the exchanged Sb and of the As vacancy on a Ga site ($GaSb_{1-y}$), respectively. According to the proposed chemical model, the different temperature dependences observed for the reaction for As_4 and As_2 species implies different reaction pathways. For both species, the final products are $GaAs_ySb_{1-y}$ and $AsSb_y$ that form in steps (3) + (6) and (4) + (5) in the case of As_2 and As_4, respectively. Furthermore, these reaction pathways offer an explanation for the different concentrations of the reaction products of the exchange and $AsSb_y$ formation for the As_2 and As_4 species. In particular, for the As_2, the larger $GaAs_ySb_{1-y}$ formation results from the first order kinetics being $k_{exch} > k_r$. For the As_4 species, the observed temperature dependence through a maximum for the $GaAs_ySb_{1-y}$ formation could be explained by applying the formalism of the topochemical reactions for a second order kinetics, i.e.

$$\frac{d\left[GaAs_ySb_{1-y}\right]}{dt} = k_{iso} \cdot k_r^{'} \cdot \theta_{As}^2 \cdot S_{GaSb} \qquad (19)$$

where Θ_{As} is the coverage of As at the reactive interface and S_{GaSb} is the GaSb surface area available for the anion exchange. The above equation takes into account the different temperature dependence of the k_{iso} and k_r' rate constants, and of the Θ_{As} as well.

Previous studies [27] have reported that As for Sb exchange is self-limiting because after a few monolayers of GaAs formation, further exchange is inhibited. According to the proposed model, the explanation of the self-limiting nature is the interface segregation of $AsSb_y$ that acts as a sink for As, and reduces S_{GaSb}. This competition between AsSby formation and anion exchange may explain reports of disordered, defective, and phase separated GaAs/GaSb superlattices using As_4, while structures grown with As_2 show improved crystalline quality.

The case of P/As exchange is examined in the context of surface reconstruction and associated As population. The experimental results presented above indicate that an increased surface population of As acts as a barrier to the formation of GaP_yAs_{1-y}. Therefore, P-for-As exchange is best described in terms of the concomitant and competitive reactions of both As and Ga with incident P. The rates of these two reactions determine the rate of the overall process and the composition of the layer created by phosphorus in-diffusion. In addition, the reactions depend on the temperature. In order to clarify these effects, we begin from a consideration of the different factors controlling the reactivity of the P and As. From a thermodynamic point of view, AsP (4.49 eV) and GaP bond strengths (2.38 eV) are higher than GaAs (2.17 eV). Hence, the higher chemical stability of products is the driving force for the reaction. In the temperature range investigated, the desorption rate constant of arsenic is much smaller than that of phosphorus. The activation energies for arsenic and phosphorus desorption from GaAs and GaP are 2.5 eV and 1.86 eV, respectively [27]. The diffusion coefficient of P into GaAs (10^{-7}-10^{-8} cm^2s^{-1}) is higher than the self-diffusion coefficient of As in GaAs [28]. This means that the P in-diffusion is very fast and not rate limiting. Given, the lower coefficient of self-diffusion of As in GaAs, through vacancies that are saturated with in-diffusing phosphorus, the out-diffusion of As could be a slow process. However, we do not observe by XPS or SE any interface segregation of As resulting from the P-for-As anion exchange. From this, it can be inferred that P can easily react with As either in the solid or on the surface at temperatures yielding PAs, which has a high vapour pressure. On the basis of the earlier considerations, we can begin to outline a chemical model for P-for-As exchange at GaAs surfaces. The model should include the supply of P to the GaAs surface where P adsorbs and the chemical barrier effects of the surface excess of As. We will assume a surface reactive step involving the As and the P, yielding volatile AsP that getters As from the GaAs surface and makes Ga sites available for exchange. Due to the fast P in-diffusion into GaAs, P for As exchange proceeds through the bulk to yield GaP bond formation, and As atom can slowly diffuse outward and/or react quickly with P yielding PAs. All the above steps can be included in the following chemical model for the P for As interactions:

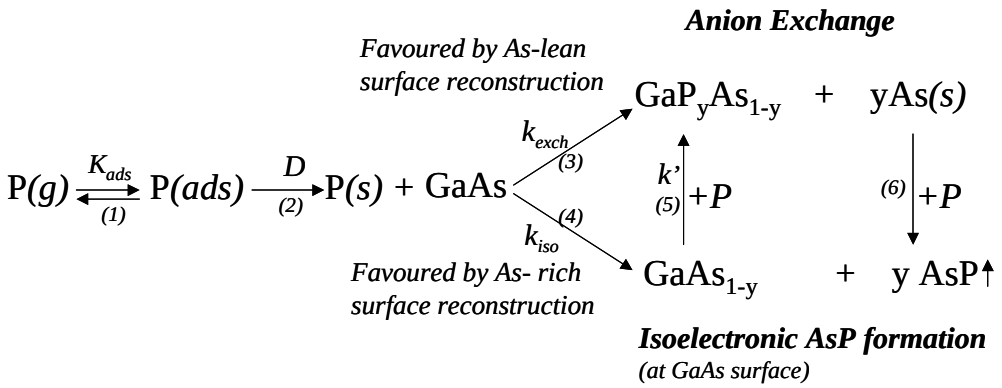

(20)

where K_{ads} is the chemsiorption constant for P atoms, D is the diffusion coefficient for the in-diffusion of P atoms, k_{exch} and k_{iso} are the true rate constants of the reactive step at the GaAs surface yielding anion exchange and an As-vacancy by isoelectronic formation, respectively and k' is the rate constant for the reaction of P with the As vacancy on a Ga site ($GaAs_{1-y}$) yielding the ternary GaP_yAs_{1-y} compound. According to the above chemical model, the formation of $GaP_yAs_{1-y,}$ occurs through a first order kinetics on the As-lean GaAs, while it is a two step reaction on the As-rich GaAs. Thus, the above experimental data have shown that, independent of As surface reconstruction of GaAs, the P for As exchange process is not controlled by the P diffusion. This indicates that the reactive step (3-4) takes place in the kinetic regime, i.e., the rate of the reactive step depends on the GaAs sites available for P adsorption. Hence, an excess of As inhibits the formation of GaP_yAs_{1-y} by scavenging P through the formation of PAs.

2.3. Hybrid Neural Network Modeling of Anion Exchange

Using some simplifying assumptions, a hybrid neural network model was constructed by characterizing the growth of $GaAs_{1-y}P_y$/GaAs strained layer superlattices (SLS) grown on (001) GaAs substrates by molecular beam epitaxy. These heterostructures were formed by the P_2 exposure of an As-stabilized GaAs surface, and *ex-situ* high resolution x-ray diffraction (HRXRD) was performed to determine the phosphorus composition at the interfaces. A first-order kinetic model was then developed to describe the mechanisms of anion exchange, surface desorption, and diffusion. A semi-empirical hybrid neural network was used to estimate the parameters of the kinetic model and analyze the microscopic processes occurring at the interfaces of the mixed anion III-V heterostructures. The phosphorus diffusion process in GaAs was estimated to have a diffusion coefficient of $D = 7\times10^{-15} \exp(-0.11/k_BT_s)$ cm^2s^{-1} for samples with $P_{As_4} = 4\times10^{-6}$ torr and exhibited enhanced phosphorus intermixing for samples with lower As-stabilizing fluxes.

The investigation proceeded by conducting a D-optimal experiment designed to systematically characterize the growth of 10-period $GaAs_{1-y}P_y$/GaAs strained layer superlattice (SLS) structures. The incorporation of phosphorus in the SLS structures was achieved by the P_2 exposure of an As-stabilized GaAs surface and an immediate overgrowth of GaAs. The D-optimal experiment implemented for this investigation provided a basis for modeling the

phosphorus composition at the interfaces of the SLS structures as a function of substrate temperature (T_s), phosphorus exposure time (t_{exp}), and As-stabilizing flux. The growth conditions and factor settings for the D-optimal experiment are provided in the Table 2.3.1 below.

Table 2.3.1: P-for-As Anion Exchange Experimental Design

Factor Description	Symbol	Settings
Substrate Temperature	T_s	420 to 520°C
P_2 Exposure Time	t_{exp}	10 to 50s
P_2 Exposure Flux (BEP)	P_{P_2}	4.5×10^{-6} Torr
As_4 Stabilizing Flux (BEP)	P_{As_4}	2×10^{-6} Torr, 4×10^{-6} Torr

Growth was performed on undoped (001) GaAs epi-ready substrates in a Riber 2300 solid-source molecular beam epitaxy system equipped with a valved As cracker and a three-zone valved P cracker. The surface reconstructions at the interfaces of the SLS structures were observed during P_2 exposure of GaAs using *in-situ* reflection high-energy electron diffraction (RHEED). The phosphorus composition present at the interfaces of the $GaAs_{1-y}P_y$/GaAs SLS structures was determined by performing standard HRXRD $\theta/2\theta$ linescans around the substrate (004) reflections.

The following kinetic model was derived to quantitatively describe the microscopic processes that occur during the complete growth sequence for the SLS structures.

$$y(T_s, t_{exp}, \Phi) = s\Phi\tau\left[1 - \exp\left(-t_{exp}/\tau\right)\right] \times \left[1 + 2\sqrt{Dt_{exp}/\pi}\right] \tag{21}$$

A semi-empirical hybrid neural network was subsequently developed that incorporates this first-principles kinetic model with a multilayer feed-forward perceptron neural network. The hybrid neural network designed to predict anion intermixing for the GaAsP/GaAs heterostructures is illustrated below. The neural network component of the hybrid model has the MBE process conditions as its inputs. The outputs of the neural network component are the unknown parameters required to implement the kinetic model.

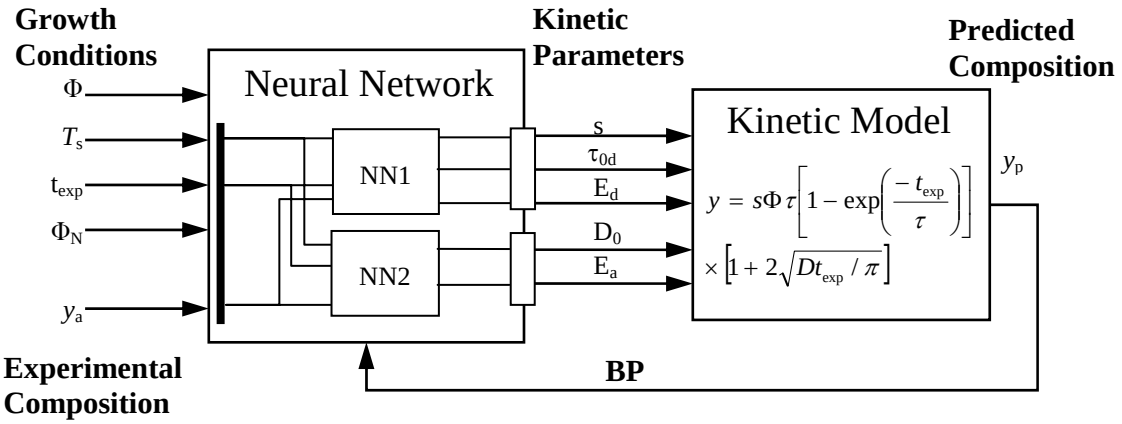

Figure 2.3.1: Hybrid neural network used to estimate the kinetic parameters for growth of the As/P heterostructures.

Evaluation of the hybrid neural network model was performed in terms of the root mean squared error (RMSE). The hybrid neural network implemented for samples with an As-stabilizing flux P_{As4} = 4×10^{-6} Torr demonstrated a training RMSE of 0.028% and a prediction RMSE of 0.574%. The figure below illustrates the measured phosphorus composition versus the predicted composition for these samples, indicating the accuracy of the hybrid neural process model.

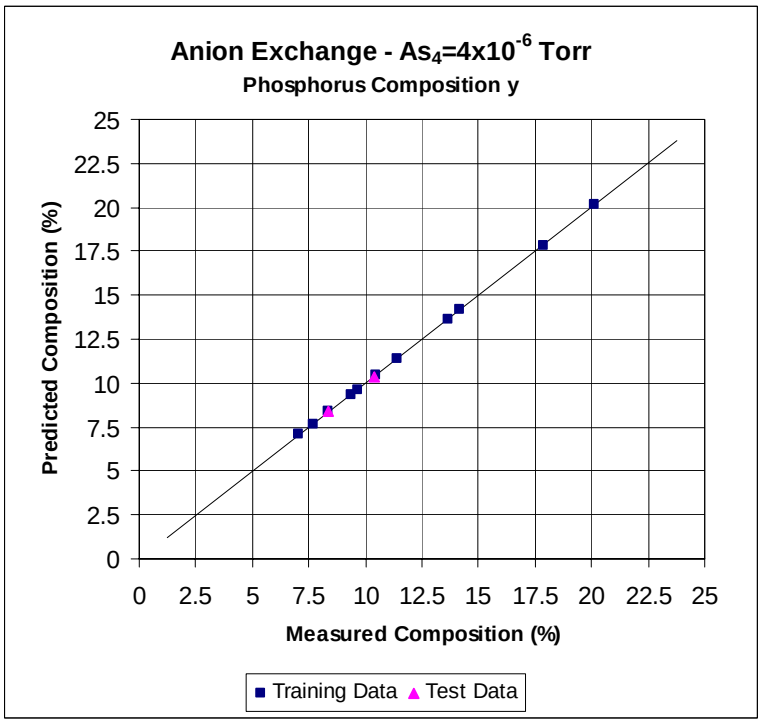

Figure 2.3.2: Experimental phosphorus composition versus neural network predictions for As_4 = 4×10^{-6} torr.

Similar results were obtained for the samples with an As-stabilizing flux $P_{As4} = 2\times10^{-6}$ torr. The measured phosphorus composition versus the predicted composition for these samples is illustrated in the figure below. The kinetic parameters derived are provided in Table 2.3.2. Using these estimated parameters, the hybrid model can predict the phosphorus composition of the mixed arsenic/phosphorus III-V heterostructures accurately.

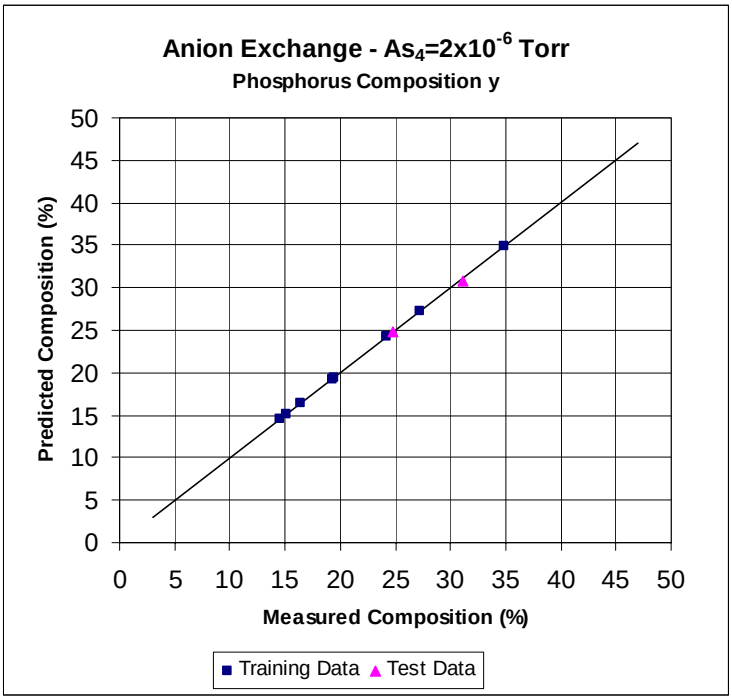

Figure 2.3.3: Experimental phosphorus composition versus neural network predictions for $As_4 = 2\times10^{-6}$ torr.

The hybrid model is important for analyzing the microscopic processes occurring at the interfaces of the GaAsP/GaAs heterostructures. Several fundamental relationships are evident upon comparing the kinetic parameters for the two distinct As-stabilizing fluxes. The higher As flux corresponds to atomic surface structures with increased surface arsenic coverage. It is apparent from the model predictions that the phosphorus sticking coefficient for samples with $P_{As_4} = 4\times10^{-6}$ torr is smaller than those with $P_{As_4} = 2\times10^{-6}$ torr. This is due to the relative increase in As surface coverage corresponding to stable surface structures such as the c(4×4) reconstruction. Experimental estimates of group V sticking coefficients predict values ranging from 0.25 to 0.75 cm^2. The sticking coefficient of P_2 on the (001) GaAs surface is at a maximum when the group-III is present on the surface. Therefore, the phosphorus sticking coefficient values of ~0.36 cm^2 obtained correspond well to the non-growing (no incident group-III) anion exposure conditions.

Table 2.3.2: Kinetic parameters from neural network model.

Kinetic Parameters – As_4 = 4×10^{-6} Torr					
s	τ_{0d}	E_d	D_0		E_a
(cm^2)	(s)	(eV)	(mol/s)	(cm^2/s)	(eV)
0.358	6.412	2.985	17.358	7×10^{-15}	0.11
Kinetic Parameters – As_4 = 2×10^{-6} Torr					
s	τ_{0d}	E_d	D_0		E_a
(cm^2)	(s)	(eV)	(mol/s)	(cm^2/s)	(eV)
0.369	3.665	2.427	26.994	1×10^{-14}	0.05

For phosphorus surface desorption, a lower activation energy and increased reaction frequency (shorter surface lifetime) were observed for the P_{As_4} = 2×10^{-6} torr samples. These results indicate an increase in phosphorus desorption for the P_{As_4} = 2×10^{-6} torr samples. It should be noted that a decrease in As pressure results in a less As-rich surface, and group V desorption begins to occur at lower substrate temperatures. Therefore, the α phase of the GaAs (001)-(2×4) surface structure, obtained at T_s = 520 °C for the P_{As_4} = 2×10^{-6} torr samples, has increased group-V desorption compared to the β(2×4) surface structure, present at T_s = 520 °C for the P_{As_4} = 4×10^{-6} torr samples. These results support the theory that surface desorption is governed by the species of atoms and their orientation (i.e., reconstruction) on the surface and contributes to the characteristic nonlinear behavior of group V incorporation.

2.4. InAs-AlSb HEMT Structures: Impact of Inverted Interface Formation

The InAs-AlSb high electron mobility transistor (HEMT) is of critical importance for future millimeter wave and high speed electronic devices. We have achieved record 300K electron mobility in InAs channel structures. We have applied various growth techniques to the critical mixed-anion, As/Sb, inverted interface to discover the impact on device-relevant properties.

Experiments were performed so that the effect of growth conditions on the interface formation could be examined. The statistically designed experiment conditions and results are provided in Table 2.4.1. Disregarding the outlier, these experiments produced test structures with average 300 ºK mobility above 20,000 cm^2/V/s. They also produced low temperature mobility that encompassed a range of 90,000 cm^2/V/s.

Table 2.4.1: 300 °K and 77 °K Mobility Results

INDIUM BARRIER (Å)	CHANNEL TEMP = 460 °C+	77 ºK MOBILITY ($cm^2/V/s$)	300 ºK MOBILITY ($cm^2/V/s$)
15	-15	95038	24773
3	30	106792	29356
17.48	7.5	135367	24259
15	30	80257	25716
3	-15	91439	28520
9	39.31	98921	24797
1.3	7.5	101738	31954
9	7.5	137729	28188

Neural network process models were developed for each response. Growth conditions (temperature, indium barrier thickness) were inputs to the neural network, and the responses (electron mobility at 300 ºK and 77 ºK) were outputs. The network structures and results are provided in Table 2.4.2. Plots of the growth conditions and responses generated by the process models are provided in Figure 2.4.1.

Table 2.4.2: Growth condition process models

	GC 300 ºK	GC 77 ºK
NN Structure	2-2-1	2-2-4-1
Training error (%)	0.23	0.48
Testing error (%)	5.35	6.55

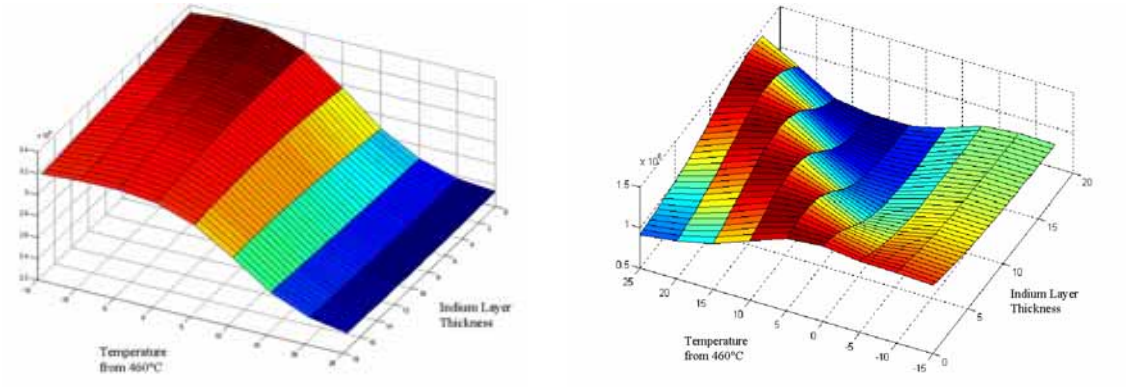

(a) (b)

Figure 2.4.1: Models based on growth conditions (a) 300 °K mobility (b) 77 °K mobility

It is well known that In-Sb bond formation must be forced at the inverted interface of InAs-AlSb in order to achieve high mobility in the InAs channel. The reasons for this are still somewhat unclear, although clues suggest that exchange and segregation play a key role. Therefore we choose to investigate the conditions of substrate temperature, which is intimately related to segregation and exchange, and In deposition on the Sb-saturated AlSb surface. The room temperature mobility model derived from the experimental data indicates a strong correlation with substrate temperature. The electron mobility is inversely proportional to substrate temperature during formation of the interface. Conversely, the deposited indium thickness does not appear to have an effect on the room temperature mobility. Depositing multiple monolayers of indium at the interface seems illogical since it leaves the interface metal rich, except the results do not invalidate these experiments. It may be that room temperature electron transport measurements are not sensitive enough to explore the impact of both indium and temperature on the interface formation. However, it is certain that substrate temperature plays a role in the amount of indium retained on the growth surface, ie. some of the InSb may well be desorbed from the surface thereby modifying the Sb/As profile at the interface.

Low-temperature electron transport is sensitive to the quality of the interface [29]. Interfacial roughness scattering has been responsible for the decrease in electron mobility at low temperature. The low-temperature electron transport presented demonstrate a correlation with both temperature and indium deposition. The low-temperature model (Fig. 26b) reveals maximums in two particular regions: (1) more indium deposited at higher temperature, and (2) thinner indium layer at lower temperature. It is possible that there is little difference in the quality of the interface between these two regions. In region (1), indium desorbs at higher temperatures, thus creating an interface similar to those formed in region (2). However, when the indium barrier is thick at lower temperature, multiple layers of indium can exist, which are converted to InAs by the ensuing As flux. The model also illustrates that when the indium barrier is thin, low temperature mobility is inversely proportional to increasing temperature,

suggesting that interface is affected, possibly roughened, as indium desorbs from the surface. When indium is desorbed so as not to protect the underlying Sb layer, anion exchange can occur, thus creating AlAs-bonds at the interface. The low-temperature model is effective in illuminating indium's role as a function of substrate temperature on interface formation.

3.0. PUBLICATIONS

3.1. Journal Articles

[1] A. Brown, M. Losurdo, G. Bruno, T. Brown, and G. May, "Fundamental Reactions Controlling Anion Exchange During the Synthesis of Sb/As Mixed Anion Heterojunctions," *J. Vac. Sci. & Tech. B*, vol. 22, no. 4, Jul/Aug, 2004.

[2] T. Brown, G. May, and A. Brown, "Hybrid Neural Network Modeling of Anion Exchange at the Interfaces of Mixed Anion III-V Heterostructures grown by Molecular Beam Epitaxy," submitted to *IEEE Trans. Semi. Manufac.*, Aug., 2004.

[3] Maria Losurdo, Pio Capezzuto, Giovanni Bruno, April Brown, Terence Brown, Gary May," Fundamental Reactions Controlling Anion Exchange During Mixed Anion Heterojunction Formation: Chemistry and Kinetics of Sb-for-As and As-for-Sb Exchange Reactions," submitted to Physical Review B.

[4] April S. Brown, Maria Losurdo, Pio Capezzuto, Giovanni Bruno, Terence Brown, and Gary May, "Fundamental Reactions Controlling Anion Exchange During Mixed Anion Heterojunction Formation: Chemistry and Kinetics of P-for-As Exchange Reactions," submitted to Physical Review B.

[5] G. Triplett, G. May, and A. Brown, "Modeling Electron Mobility in MBE-Grown InAs/AlSb Thin Films for HEMT Applications Using Neural Networks," *Solid State Electronics*, vol. 46, no. 10, pp. 1519-1524, Oct., 2002. (also supported by DARPA ABCS Program)

[6] T. Brown, A. Brown, and G. May, "Anion Exchange at the Interfaces of Mixed Anion III-V Heterostructures Grown by Molecular Beam Epitaxy," *J. Vac. Sci. & Tech. B*, vol. 20, no. 4, July/August,, 2002.

[7] Y. Wang, Z. Wang, T. Brown, A. Brown, and G. May, "Thermodynamic Analysis of Anion Exchange During Heteroepitaxy," *J. Crystal Growth*, vol. 242, p. 5, 2002.

[8] Y. Wang, Z. Wang, T. Brown, A. Brown, and G. May, "Interfacial Roughening in Lattice Matched GaInP/ GaAs Heterostructures, *Thin Solid Films*, vol. 397, p. 162, 2001.

[9] Y. Wang, Z. Wang, T. Brown, A. Brown, and G. May, "Lateral Compositional Modulation in Lattice-Matched GaInP/GaAs Heterostructures," *J. Elec. Mat.*, vol. 29, no. 12, pp. 1372-1379, Dec., 2000.

[10] Y. Wang, Z. Wang, T. Brown, A. Brown, and G. May, "Configurations of Misfit Dislocations at Interfaces of Lattice-Matched GaInP/GaAs Heterostructures," *Appl. Phys. Let.*, vol. 77, pp. 223-225, 2000.

[11] Y. Wang, Z. Wang, T. Brown, A. Brown, and G. May, "A New Misfit Dislocation Configuration at Interfaces of Lattice-Matched GaInP/GaAs Heterostructures," *Appl. Phys. Lett.*, July 10, 2000.

4.2. Conference Proceedings

[1]M. Losurdo, D. Giuva, P. Capexxuto, G. Bruno, T. Brown, G. Triplett, G. May, and A. Brown, "A Study of Anion Exchange Reactions at GaAs Surfaces for Heterojunction Interface Control," *Proc. Materials Research Society Symposium*, vol. 799, Z2.5.1-6, 2004.

[2]T. Sarmiento and G. May, "Preliminary Study of As-for-Sb Exchange for Device Applications," *Proc. International Semiconductor Device Research Symposium*, Washington, DC, Dec., 2003, pp.42-43.

[3]G. Triplett, A. Brown, and G. May, "Using Neural Networks for RHEED Modeling of Interfaces in AlGaSb-InAs HEMT Devices," *Proc. International Conference on Compound Semiconductor Manufacturing Technology*, San Diego, CA, Apr., 2002, pp. 157.

[4]Y. Wang, Z. Wang, T. Brown, A. Brown, and G. May, "Dislocation Dipole Configuration in GaInP/GaAs Heterostructures," *MRS*, Fall, 2000.

4.3. Seminars and Conference Presentations without Proceedings

[1]G. Triplett, G. May, and A. Brown, "Interrelationships in the Electronic and Structural Characteristics of AlGaAsSb-InAs HEMT Structures," *45th Elec. Mat. Conf.*, Salt Lake City, UT, June, 2003.

[2]A. Brown, M. Losurdo, G. Bruno, T. Brown, and G. May, "A Chemical and Kinetic Study of P-for-As Anion Exchange Reactions in GaAs/GaAsP Superlattice Structures, *45th Elec. Mat. Conf.*, Salt Lake City, UT, June, 2003.

[3]G. Triplett, G. May, and A. Brown, "The Impact of the Inverted Interface (InAs-on-AlSb) on InAs/AlSb High Electron Mobility Transistor Structures Grown by Molecular Beam Epitaxy," *Workshop on Compound Semiconductor Materials & Devices*, Atlanta, GA, February, 2003.

[4]M. Losurdo, G. Bruno, T. Brown, G. May, and A. Brown, "Anion Exchange Reactions and Isoelectric AsSb Formation: GaSbyAs1-y/GaAs and GaAsySb1-y/GaSb Superlattice Interface Quality," *44th Elec. Mat. Conf.*, Santa Barbara, CA, June, 2002.

[5]T. Brown, G. May, A. Brown, M. Losurdo, M. Giangregorio, P. Capezzuto, and G. Bruno, "Characterization of Anion Exchange for Mixed Group V Heterostructures during Molecular Beam Epitaxy," *44th Elec. Mat. Conf.*, Santa Barbara, CA, June, 2002.

4.0 REFERENCES:

1. M. Yano, H. Yokose, Y. Iwai, and M. Inoue, J. Crystal Growth **111**, 609 (1991).
2. M. W. Wang, D. A. Collins, T. C. McGill, and R. W. Grant, J. Vac. Sci. Technol. **B11**, 4118 (1993).
3. J. M. Moison, M. Bensoussan, and F. Houzay, Phys. Rev. B **34**, 2018 (1986).
4. G. Hollinger, D. Gallet, M. Gendry, C. Santinelli, and P. Viktorovitch, J. Vac. Sci. Technol. **B8**, 832 (1990).
5. R. Shioda, H. Oyanagi, Y. Kuwahara, and Y. Takeda, Jpn. J. Appl. Phys. **33**, 5623 (1994).
6. I. Barin, *Thermochemical Data of Pure Substances* (VH, Weinheim, 1989).
7. D. T. J. Hurle, J. Phys. Chem. Solids **40**, 613 (1979).
8. C. Pupp, J. J. Murray, and R. F. Farrow, J. Chem. Thermodynamics **6**, 123 (1974).
9. G. Castellan, *Physical Chemistry* (Addison-Wesley Publishing, Massachusetts, 1971).
10. G. B. Stringfellow, J. Cryst. Growth **58**, 194 (1982).
11. R. F. C. Farrow, J. Phys. D: Appl. Phys. **7**, 2436 (1974).
12. M. B. Panish and J. R. Arthur, J. Chem. Thermodynamics **2**, 299 (1970).
13. S. V. Ivanov, A. A. Boudza, R. N. Kutt, N. N. Ledentsov, B. Y. Mel'tser, S. S. Rumivov, S. V. Shaposhnikov, and P. S. Kop'ev, J. Cryst. Growth **156**, 191 (1995).
14. N. N. Ledentsov, Springer Tracts in Modern Physics **156**, 1 (1999).
15. C. T. Foxon, Acta Electron. **21**, 139 (1978).
16. C. Pupp, J. J. Murray, and R. F. Pottie, J. Chem. Thermodynamics **6**, 123 (1974).
17. M. Yoshida, and K. Watanabe, J. Electrochem. Soc. **132**, 1733 (1985).
18. G. X. Qian, R. M. Martin, and D. J. Chadi, Phys. Rev. B **37**, 1303 (1988).
19. M. Yano, HJ. Yokose, Y. Iwai, and M. Inoue, J. Vac. Sci. Technol. **B7**, 199 (1989).
20. R. Kaspi, J. Cryst. Growth **201/202**, 864 (1999).
21. Z. Sobiesierski, D. I. Westwood, P. J. Parbrook, K. B. Ozanyan, M. Hopkinson, and C. R. Whitehouse, Appl. Phys. Lett. **70**, 1423 (1997).
22. D. A. G. Bruggemann, Ann. Phys. (Leipzig) **24**, 636 (1935).
23. M. Losurdo, D. Giuva, M. M. Giangregorio, G. Bruno, and A. S. Brown, Thin Solid Films (2004).
24. A. S. Brown, G. Triplett, and G. May, unpublished.
25. R. Beadry, S. P. Watkins, X. Xu, and P. Yeo, J. Appl. Phys. **87**, 7838 (2000).
26. K. J. Kim, M. H. Lee, J. H. Bahng, K. Shim, and B. D. Choe, J. Appl. Phys. **84**, 3696 (1998).
27. B. W. Liang and C. W. Tu, J. Cryst. Growth **128**, 538 (1993).
28. G. C. Jain, D. K. Sadana, and B. K. Das, Solid State Electronics **19**, 731 (1976).
29. G. Triplett, A. Brown and G. May, J. Cryst. Growth **265**, 47 (2004).